AN ABSTRACT OF THE THESIS OF

Claus H. Weigand for the degree of Master of Science in Electrical & Computer Engineering presented on May 5, 1986

Title: Voltage Controller for a Variable Speed Generation System

Abstract approved: Redacted for Privacy
W. Kolodziej

An important task of a Variable Speed Generation (VSG) system is the capability to maintain and control the terminal voltage at some desired value as determined by the reactive power dispatch strategy.The main objective is to design a sub-optimal fixed-parameter controller in the sense that constraints with respect to practical operation policy, cost and reliability of the actual controller elements may outweigh the results of an optimal design based on the system response. Inspite of the nonlinear characteristics of the system it has to be effective over the entire range of operation.

The general equations for the doubly-excited machine are derived and the critical mode of operation is identified. A minimum-order transfer function is established which facilitates a convenient method to design the desired controller. The effectiveness of the designed controller as implemented to the complete VSG system is verified.

Voltage Controller
for a
Variable Speed Generation System

by

Claus H. Weigand

A THESIS

submitted to

Oregon State University

in partial fulfillment of
the requirements for the
degree of

Master of Science

Completed May 5, 1986

Commencement June 1986

APPROVED :

Redacted for Privacy

Assistant Professor in charge of major

Redacted for Privacy

Head of department of Electrical & Computer Engineering

Redacted for Privacy

Dean of Graduate School

Date thesis is presented May 5, 1986

Typed by Claus H. Weigand

ACKNOWLEDGEMENTS

I wish to express my thanks to

Professor Hian K. Lauw for his helpful assistance,

Oregon State University for accepting me as a participant of the academic exchange program between the State of Oregon and the State Baden-Wuerttemberg, Federal Republic of Germany,

and to

the Fulbright Commission, Bonn, Federal Republic of Germany, for their additional financial support.

Claus H. Weigand

TABLE OF CONTENTS

LIST OF FIGURES

LIST OF FIGURES (continued)

LIST OF FIGURES (continued)

LIST OF TABLES

Voltage Controller
for a
Variable Speed Generation System

Chapter I: INTRODUCTION

A Variable Speed Generation (VSG) system basically consists of a doubly-excited machine, a turbine supplying the mechanical input power, a power electronic converter supplying the required excitation waveforms which is controlled by a set of local controllers, and a supervisory controller.

The significant difference between the widely used Fixed Speed Generation system and a VSG system is the capability of the VSG system to supply a controllable terminal voltage of fixed frequency to the power grid irrespective of varying mechanical speeds. This capability makes the VSG system highly suitable to exploit erratic energy sources such as water and wind energy where the maximum efficiency operating condition is highly dependent on the mechanical speed of the turbine. The VSG system is capable of tracking the maximum efficiency operating condition under varying resource and electric power demand conditions.

However, steady-state operation of the doubly-excited machine requires that rotor and stator magnetic fields rotate at the same speed. Therefore the frequency of the stator current must be equal to the sum of the frequency of the rotor current and the mechanical speed of the rotor, expressed in electrical degrees, if the phase sequences of rotor and stator windings are equal.

The basic reason that VSG systems were not widely used so far was the crucial problem of supplying the rotor of the doubly-excited machine with currents of varying frequency as determined by the supervisory control logic. Research done earlier showed that the doubly-excited machine, if supplied at its rotor windings by voltage sources of variable frequency such as synchronous machines or conventional electronic power converters, turns out to be unstable for all but very small relative deviations from synchronous speed. However, the development of new and faster power switching devices in solid state technology meanwhile made the design of suitable electronic power converters possible which meet the crucial requirements of the doubly-excited machine. The quite promising capabilities of the series-resonant converter [1] should be mentioned here as a key element to the successful operation of the VSG system.

Besides the general requirement to maintain a constant utility grid voltage, the controllability of the stator terminal voltage is necessary in order to generate reactive power with the VSG system.

In Part II of this thesis mathematical models in general form are derived for the VSG system as far as it is necessary to find criteria for the validity of a linear model of the VSG system.

Part III presents the approximation of the VSG system with a linear model and a discussion of the techniques used for this purpose.

Using this linear model the approach for designing the controller is described in Part IV. Practical constraints imposed to the controller will affect the design process. Consequently, a fixed-parameter controller with a non-complex structure will be designed. Constraints with respect to cost and reliability of the designed controller will be satisfied simultaneously.

Finally, in Part V the designed controller will be implemented to the simulated VSG system and its effectiveness will be verified over the entire range of operation of the VSG system. It will be demonstrated that the controller is effective even for the most critical point of operation.

Chapter II: MATHEMATICAL MODEL OF THE VSG SYSTEM

II.1 Introduction

A detailed description of the VSG system will be presented in this chapter. Aspects of the interaction with adjacent systems will be discussed, followed by the description and analysis of the VSG system itself. The general equations of the doubly-excited machine will be derived as far as it is necessary in order to find evaluation criteria for the purpose of establishing an adequate linear model of the VSG system. Finally the interaction between the VSG system, the local controllers and the supervisory controller will be discussed.

II.2 System configuration

Figure 2.1 shows the VSG system, its major subsystems and its connections to adjacent systems (see also [2]).

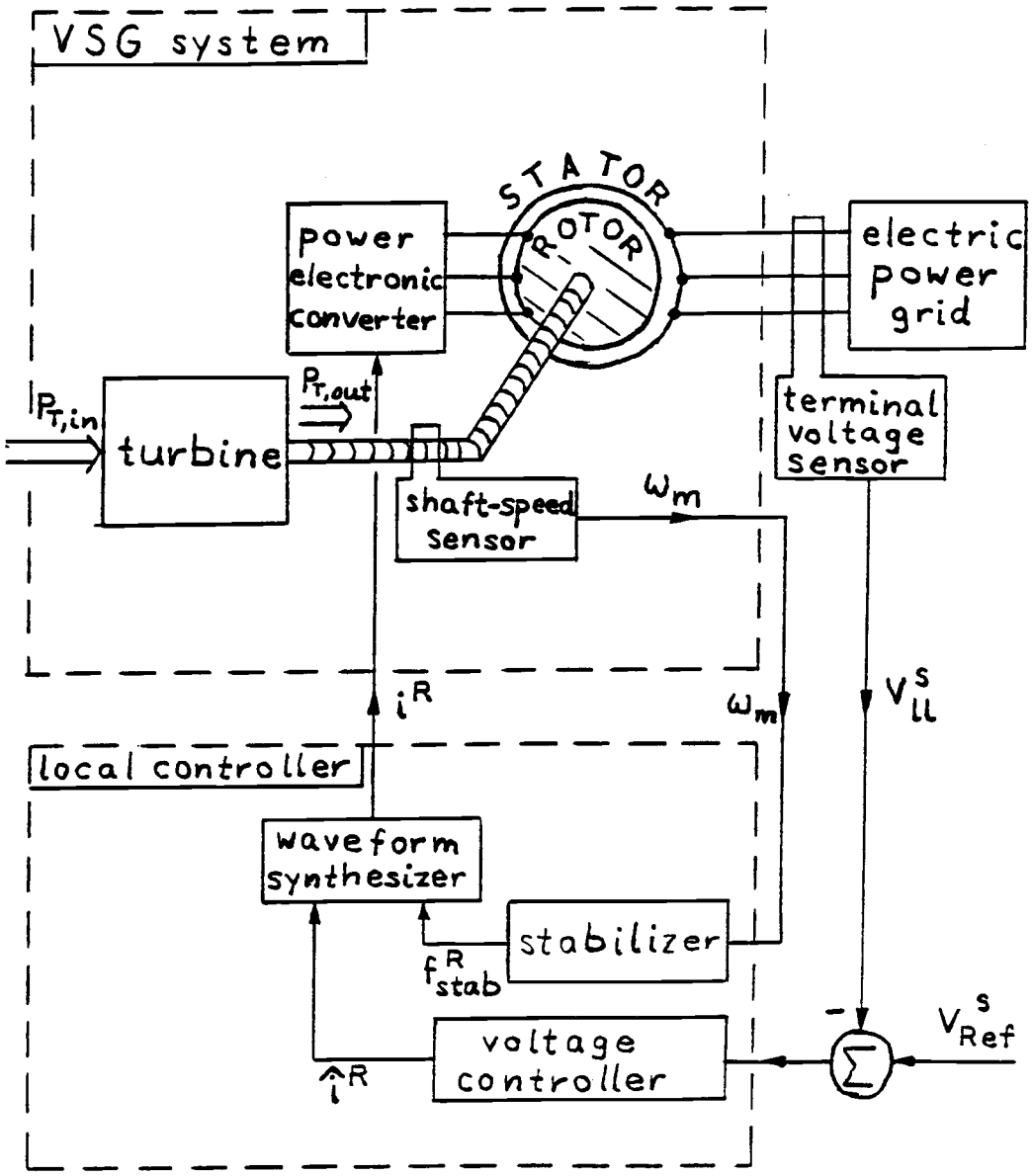

Figure 2.1 Block diagram of the VSG system

The VSG system interacts with the following adjacent systems:

a) the primary energy source $P_{T,in}$; depending on the application of the VSG system, $P_{T,in}$ is either water or wind power.

b) the electric power grid is connected to the stator terminals of the doubly-excited machine. A representation of this system with an equivalent electric circuit will be presented later.

c) the local controller which supplies the power electronic converter within the VSG system with the reference value of the rotor current i^R. It consists of the following three subcontrollers:

   i) the stabilizer which ensures stable steady-state operation of the VSG system by counteracting the tendency of the rotor speed to oscillate within a certain range.

   ii) the voltage controller; its design is the objective of this thesis

iii) the waveform synthesizer which provides the power electronic converter within the VSG system with the time-varying reference value of the rotor current i^R.

The VSG system consists of:

a) the turbine which converts the energy supplied by the primary energy source into mechanical energy,

b) the doubly-excited machine which converts the mechanical energy into electrical energy,

c) the power electronic converter supplying the rotor coils of the doubly-excited machine with the required waveform of either currents or voltages and

d) various sensors providing local controllers and the supervisory controller with necessary information from the VSG system about its actual point of operation. In order to enable the supervisory controller to perform all its required tasks, sensors for the shaft-speed of the mechanical system, for the pressure head of the turbine and for the terminal output voltage are necessary. However, for the design of the voltage controller only the sensor for the terminal output voltage is necessary.

II.3 General equations

II.3.1 Structure of the local controllers

a) The Stabilizer

The task of the stabilizer is the detection of changes in the mechanical speed ω_m of the VSG system which are due to the tendency of the rotor speed of the doubly-excited machine to oscillate. Its output signal has to compensate any speed changes. That means, if the speed increases, f^R_{stab} has to increase too and vice versa. Figure 2.2 shows the block diagram of the the stabilizer.

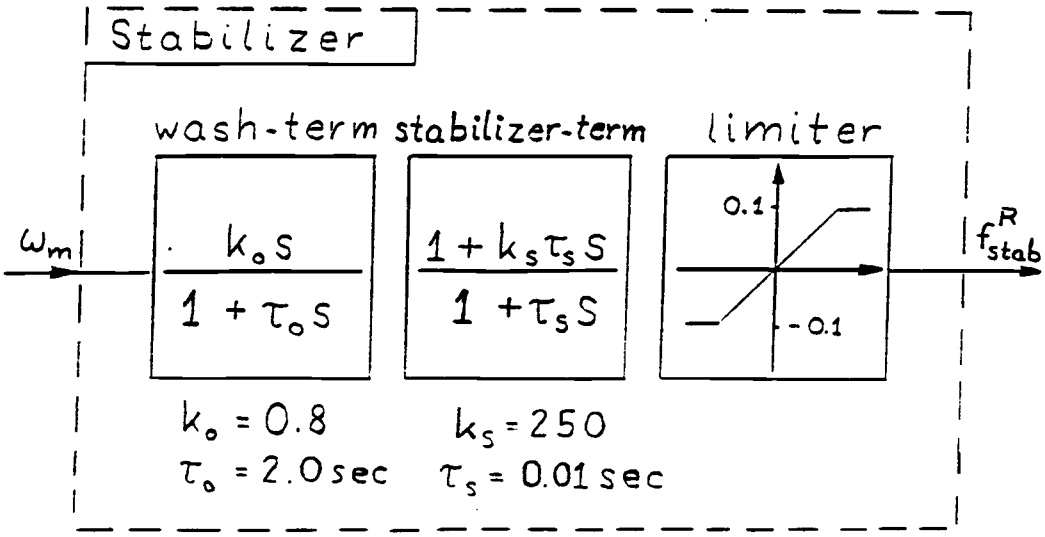

Fig 2.2 Block diagram of the stabilizer

The differentiation part of the wash-term deactivates the stabilizer if ω_m is constant. Detrimental differentiation effects are offset by a first order delay (time constant τ_o). In addition an amplification factor (k_o) is provided. The stabilizer term performs a phase shifting on the signal coming from the wash-term. The sub-optimal parameters k_o and τ_o were determined earlier by trial and error. Finally, the amplitude of the output of the stabilizer term is limited to prevent excessive rotor current frequency variations which may drag the state variables of the doubly-excited machine out of the region of attraction.

b) The Voltage Controller

The only information used by the voltage controller is the terminal output voltage of the VSG system. Its output $\hat{i}^R$ controls the rotor current amplitude of the doubly-excited machine.

c) The Waveform Synthesizer

The task of the waveform synthesizer is to synthesize the reference signal i^R for the power electronic converter. The equation for i^R is given by

$$i^R = \hat{i}^R \cos[s_o \omega^s t/100.0 + 2\pi \int_0^t f_{stab}^R(\tau)d\tau]. \qquad (2.1)$$

II.3.2 Structure of the VSG system

a) The Turbine

The task of the turbine is to convert energy from the primary energy source into mechanical energy. In the case of a water-driven generation system not only the dynamics of the turbine itself, but also the dynamics of the moving water in the penstock and reservoir and the dynamics of the mechanics controlling the turbine would have to be taken into consideration in order to obtain a model that represents the dynamics of this part of the system accurately. The mathematics involved herein soon becomes extremely elaborate since we are dealing with a system with distributed parameters requiring the solution of a system of partial differential equations. Figure 2.3 shows an approximated model of the nonlinear turbine power characteristics and penstock dynamics.

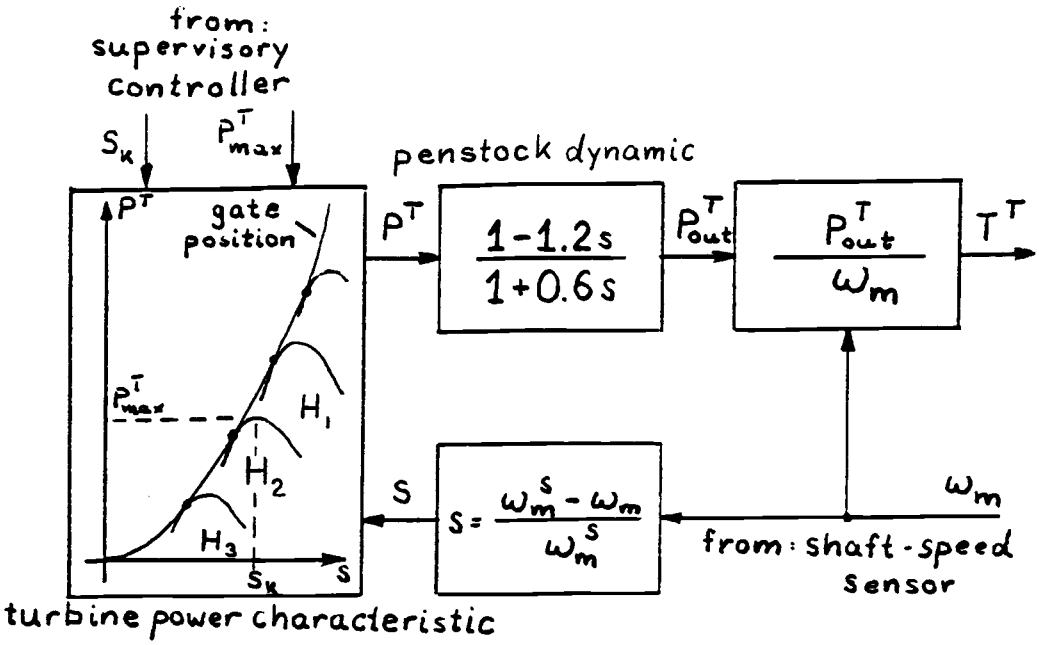

Figure 2.3 Turbine power characteristics and penstock dynamics

The turbine power characteristic is represented by the equation

$$P^T = P^T_{max} \cdot [1 - (s - s_K)^2] \ , \tag{2.2}$$

where

$$s = \frac{\omega_m^S - \omega_m}{\omega_m^S} \tag{2.3}$$

and ω_m mechanical angular speed [rad/s] ,

ω_m^S synchronous angular speed [rad/s] ,

s slip ,

s_K target slip ,

P^T_{max} maximum efficiency turbine output power [Watt]

and P^T turbine output power [Watt] .

The dynamic behavior of the penstock can be considered equivalent to that of a phase-shifter between P^T and the available output power of the turbine, P^T_{out}. T^T is the turbine output torque.

The dynamics of the mechanical system within the VSG system can be represented by the equivalent electric circuit as shown in Figure 2.4.

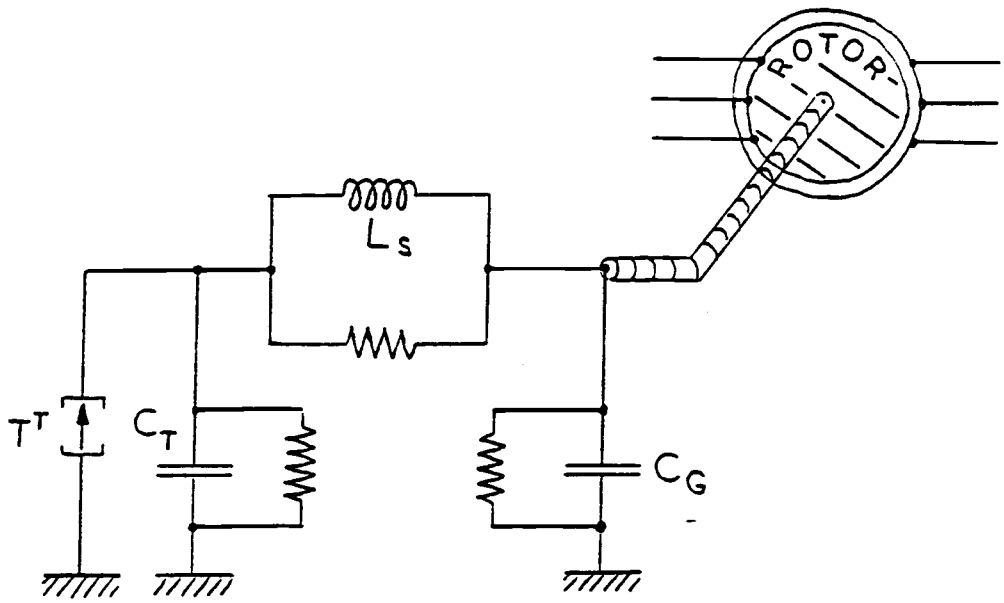

Figure 2.4 Equivalent electric circuit model for the mechanical part of the VSG system

The following notation is used:

$T^T \sim$ output turbine torque [Nm] ,

$1/L_S \sim$ stiffness of the shaft [Nm/rad] ,

$C^T \sim$ inertia of turbine rotor [Nms^2] ,

$C^G \sim$ inertia of generator rotor [Nms^2]

$(C^G >> C^T)$

and resistances account for mechanical losses.

b) The Doubly-Excited Machine

The task of the doubly-excited machine is to convert mechanical power into electric power. The machine itself is a three-phase wound rotor induction machine. The rotor windings are connected to external electric circuits through slip rings. The voltage equation for each coil is given by

$$v(t) = R \cdot i(t) + \frac{d}{dt} L(\Theta,t) \cdot i(t) \ , \qquad (2.4)$$

where Θ denotes the rotor position and satisfies the non-linear differential equation

$$\dot{\Theta} = f(\Theta, i) \ . \qquad (2.5)$$

The product term $L(\Theta,t) \cdot i(t)$ indicates the presence of a nonlinear set of differential equations. A thorough analysis continuing from this point on can be found in [3].

The complete set of state equations for electric and mechanic state variables can be written in the form

$$\dot{\underline{x}} = f(\underline{x},\underline{y},\underline{u})$$
$$\dot{\underline{y}} = f(\underline{x},\underline{y},\underline{u}) \ , \qquad (2.6)$$

where

$\underline{x}$ is a vector consisting of electric state variables,

$\underline{y}$ is a vector consisting of mechanic state variables

and $\underline{u}$ is the input vector of the system.

It can be observed that this system can be decoupled in two independent systems of electric and mechanic state variables if the rotor speed is kept constant.

c) The Power Electronic Converter

The task of the power electronic converter is to supply the three-phase rotor windings of the doubly-excited machine with current waveforms of variable amplitude and frequency such that they are proportional to the signal i^R from the waveform synthesizer and phase-shifted by $2/3\pi$ electrically with respect to each other. In its practical form the power electronic converter will synthesize the rotor currents using some kind of switching process. Due to the application of semiconductor switches (thyristors or transistors) the output currents will be highly contaminated with harmonics of the desired frequency. Consequently, all power electronic converters are provided with an output filter. The

effectiveness of an optimal controller design should be verified with a system representation which takes the filter characteristics into account. It is remarked that the series-resonant converter only requires a filter which filters out the sampling frequency. This is opposed to other converter types which require a low-order harmonics filter. Since the series-resonant converter is intended to be used as a programmable current source, it its necessary to provide the converter model with a capacitive output filter.

II.4 Complete model of the VSG system

The VSG system and its subsystems as well as the relevant parts of the local controller and other adjacent systems of the VSG system are now completely described in a general form. It needs to be mentioned that completeness is only achieved as far as necessary to cover all parts which form a dynamic system together with the voltage controller. The generation system also includes a supervisory controller. However, since this controller imposes only small and extremely slow changes on state-variables of the VSG system, their influence on the dynamic behavior of the system can be practically assumed to be negligible.

Chapter III: DESCRIPTION OF THE APPROXIMATED SYSTEM

III.1 Introduction

In Chapter II the mathematical model of the VSG system was introduced in general form. It is now obvious that a rigorous mathematical analysis of the whole system would be extremely difficult. This however would be necessary in order to design an optimal voltage controller for the system. On the other hand it can be predicted already at this stage that due to the nonlinearity of the system the designed optimal voltage controller would be optimal only for that point of operation it originally was designed for. In order to have an optimal controller for all possible points of operation an adaptive controller would be necessary. This however would complicate the controller structure. The challenge is to design a fixed-parameter controller that is easy to implement, effective for all possible points of operation, reliable, and using only the terminal voltage of the VSG system as input.

Consequently, for the design of the voltage controller a transfer function representing the VSG system with $\hat{i}^R$ as input and V_{ll}^S as output has to be established.

For the expediency of the design, it is highly desirable to establish a transfer function of minimal order which yet reflects the dynamic behavior of the terminal voltage sufficiently accurate.

The following investigation will heavily rely on the numerical simulation of the VSG system with the Electro Magnetic Transients Program (EMTP). Initially, frequency responses of the system for various points of operation will be established. The desire is to find the transfer function corresponding to the operating point which seems to be most critical to the effectiveness of the voltage controller. In the next step a transfer function will be derived based on the use of a curve fitting method both in the time domain and in the frequency domain.

An alternative approach to the frequency response technique will be presented which yields significantly improved results. Therefore two numerical methods will be introduced. The first algorithm determines the order of a dynamic system from samples of its impulse response. The second algorithm determines a more accurate transfer function of the VSG system using samples of the step response of both the VSG system and the transfer function G(s) as obtained before.

III.2 Determination of the frequency response

III.2.1 Simplification of the system for the simulation

Although it would be possible to implement the VSG system with an approximation of the dynamics of the complete mechanical system, initial steps are taken in order to simplify the system configuration.
From Figure 2.3 it can be seen that the penstock dynamics and turbine power characteristics become only relevant if changes in ω_m occur. For the process of obtaining the frequency response of the electrical part of the system, the dynamics of the mechanical part of the system can be neglected as long as changes in ω_m are kept sufficiently small. Consequently, the turbine torque is assumed to be constant.

The frequency responses will be determined as follows: A pulse of the duration of one integration step of the simulation will be applied to the input $\hat{i}^R$. The response of the terminal voltage is monitored until all transients have settled. Then a Discrete Fourier Transform will be performed on the difference signal between V_{ll}^s and its dc-component V_{Ref}^S. The resulting frequency responses will be plotted in Bode-diagrams.

III.2.2 The data case for the simulation

The data case for the determination of the frequency response now contains the following parameters of the elements of the VSG system and its adjacent systems:

a) The VSG system:

i) Data of the doubly-excited machine:

3MVA, 4.2kV, 18-pole, 400rpm

unsaturated d- and q-axis main inductance	25.72mH
leakage inductance of stator coil	1.29mH
resistance of stator coil	0.2Ω
leakage inductance of rotor coil	1.29mH
resistance of rotor coil	0.06Ω
point of operation (slip)	0.1%

frequency responses also determined for 20%, 40% and 60% slip

ii) Power electronic converter:

Controlled three-phase current sources; their actual value is equal to the reference value i^R of the waveform synthesizer and their phase is shifted by $2/3\pi$ with respect to each other.

filter capacitors (to ground)	100.0μF

iii) Turbine:

Constant current source; the value is determined by the steady-state initialization of the simulation

b) Local controller:

i) Stabilizer:

The stabilizer is implemented as s-transfer function according to Figure 2.2 with the parameters as given there.

ii) Waveform synthesizer:

The waveform synthesizer calculates the reference value of the output current i^R according to eq. (2.1) with $I^R_{Amp,0} = 707.1$ Amp.

c) Terminal voltage sensor:

The terminal voltage sensor determines V^S_{ll} by

$$V^S_{ll} = \sqrt{N^2_{Sl_a} + N^2_{Sl_b} + N^2_{Sl_c}} \quad , \qquad (3.1)$$

where N_{Sl_x} denotes stator line-to-ground voltages [Volts].

d) Electric power grid

The electric power grid is modeled as 3 voltage sources, phase-shifted by $2/3\pi$ with respect to each other, and by series resistances and impedances accounting for losses and impedances of the connecting transformers and transmission lines.

Voltage sources:

amplitude	3656.8 Volts
frequency	60.0 Hertz

Transformer:

resistance	0.031Ω
inductance	0.5875mH

Transmission line:

resistance	1.0Ω
inductance	10.0mH

III.2.3 Simulated impulse response

The general idea now is to subject the system as described above to a pulse which is superimposed on i^R and has the duration of one integration step. The following considerations determine the choice of the pulse amplitude:

a) It must not be larger than a certain value in order to suppress the influence of the system nonlinearities. This value can be found by testing the validity of the homogenity theorem of linear systems. A pulse $u_1(t)$ of a certain amplitude is applied to the system; then in a second simulation a pulse $u_2(t)$ of half the amplitude of $u_1(t)$ is applied. The requirement for approximately linear behavior of the system is that the corresponding output functions $y_1(t)$ and $y_2(t)$ compare as follows:

$$y_2(t) \cong 1/2 \cdot y_1(t)$$

Deviations of up to 10% were considered as still acceptable.

b) The pulse amplitude should be as large as possible in order to minimize the influence of rounding errors in the calculation process. The simulations revealed that a good choice for the pulse amplitude is 200.0Amp for the data case with an operation point of 0.1% slip, and 20.0Amp for the data cases with operation points of 20%, 40% and 60% slip.

III.2.4 Discrete Fourier Transform of the impulse response

The EMTP simulation software provides the option to calculate a Discrete Fourier Transform (DFT) of a previously calculated time series. The parameters for the DFT are chosen as follows:

number of DFT coefficients requested	100
duration of time series	50.0msec

Thus we obtain equidistant samples in the frequency domain between zero and 2kHz with 20Hz intervals. Note that values between samples are not defined, but interpolated in the plots [4]. Figure 3.1 shows the impulse response of the data case for a machine slip of 0.1%. Figures 3.2a,b,c,d show the frequency responses for machine slips of 0.1%, 20%, 40% and 60%.

The actual scaling of the frequency axis is in multiples of 20Hz. Thus

$$0.0 \mathrel{\hat{=}} 20\text{Hz}$$

$$1.0 \mathrel{\hat{=}} 200\text{Hz}$$

$$2.0 \mathrel{\hat{=}} 2000\text{Hz}$$

Comparing Figures 3.1 and 3.2 the presence of a strong mode at about 160Hz (8th harmonic) becomes obvious.

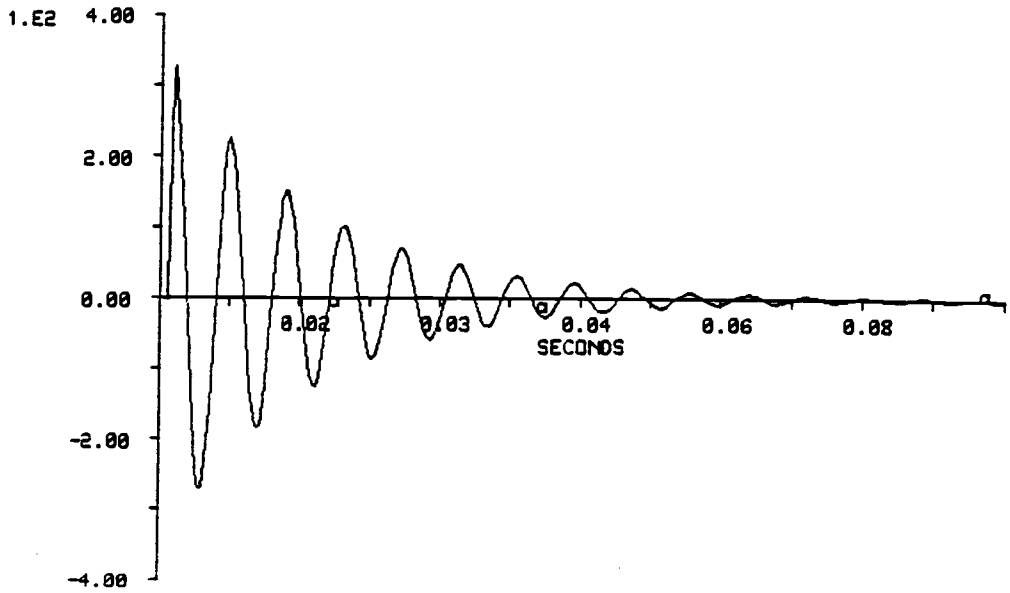

Figure 3.1 Impulse response of the VSG system

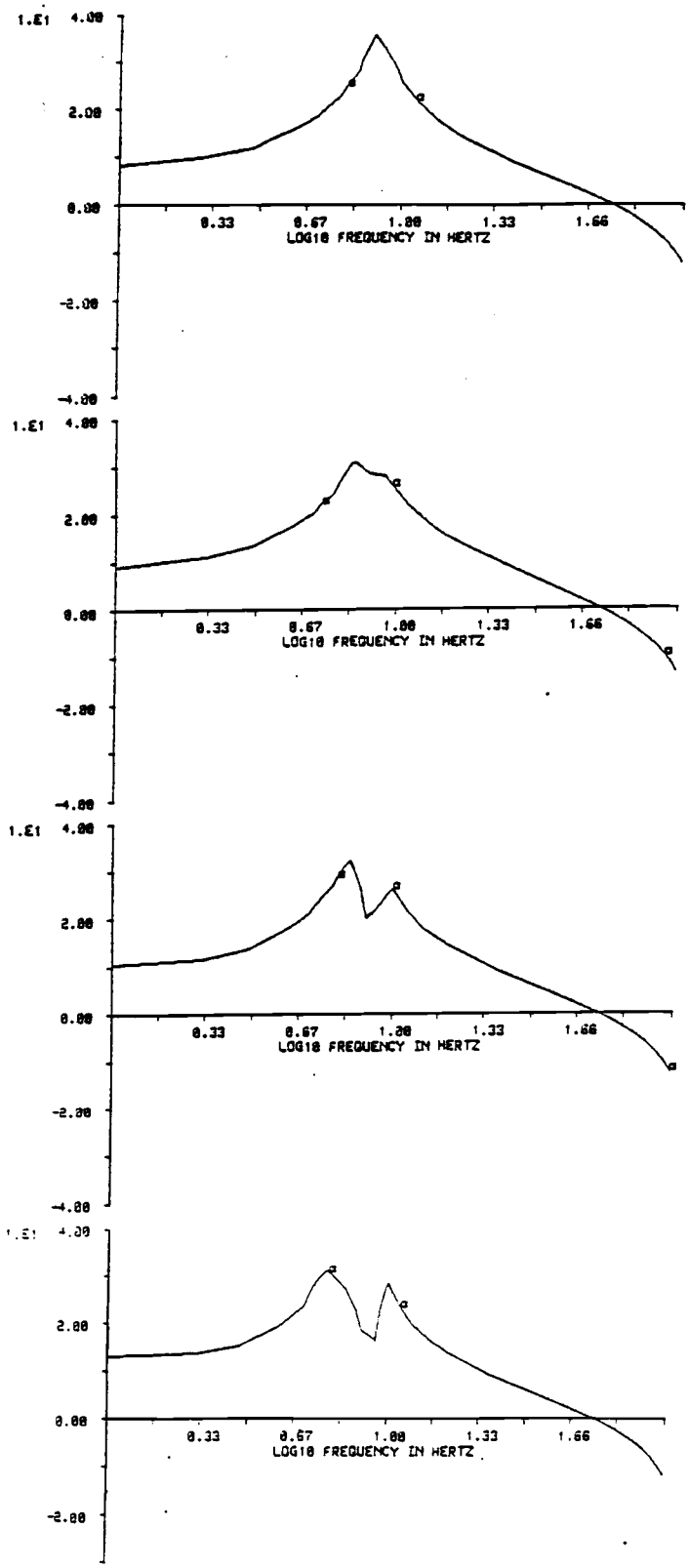

Figure 3.2

Frequency responses

of the VSG system for

a) 0.1% slip

b) 20.0% slip

c) 40.0% slip

d) 60.0% slip

III.3 Curve fitting method based on Bode-diagram

III.3.1 Choice of the most critical point of operation

Out of the previously obtained frequency responses one has to be chosen for the approximation of a transfer function for the VSG system. Out of Figure 3.2a,b,c,d the frequency response for the point of operation with the slip 0.1% (Figure 3.2a) was chosen because the extremum around 160Hz has the largest value of all responses. Consequently the corresponding dynamic behavior is suspected to be most critical of all responses as found in III.2.

III.3.2 Determination of the order of the linear system

In order to determine the order of the approximated linear system a reference is made to the block diagram of the VSG system in Figure 2.1. The following variables are state variables of the system:

a) The rotor and stator coil currents,

b) The voltages across the output filter capacitors of the power electronic converter,

c) The shaft speed of the mechanical system

In addition we have to add the order of the stabilizer transfer function which was included in the simulation.

The conclusion is that a linear system of order eight has to be considered.

III.3.3 Curve Fitting

Approximating the impulse response in Figure 3.1 with the function

$$g_1(t) = k \cdot \exp[-t/T] \sin \omega_0 t \qquad (3.2)$$

a result was obtained that matches best with the impulse response of the system, if

$$T = 13.8\text{msec}$$

and $\omega_0 = 1005.6$ 1/sec,

k will be chosen later.

This yields in the frequency domain a factor G_1 of the complete transfer function G. The Laplace transform of $g_1(t)$ is

$$G_1 = \frac{k}{s^2 + (2/T)s + (1/T)^2 + \omega_0^2} \quad . \qquad (3.3)$$

Since G is of order eight, six more poles have to be found. In Figure 3.2a the observation can be made that the slope of the frequency response is -40dB/decade for frequencies above 2kHz. Consequently, the difference between the orders of the numerator and denominator polynomial must be two. Therefore the numerator polynomial of G is of order six.

The additional poles and zeros are chosen such that they improve the approximation for the frequency response of the VSG system. Figures 3.3 and 3.4 show the Bode-diagrams of a first order zero $F_1(s) = 1 + sT$ and $F_2(s) = 1/(1 + sT)$. Therefore [5], if a pole or zero is added at a certain frequency the influence on the shape of the frequency response around that frequency is according to Figures 3.3 and 3.4.

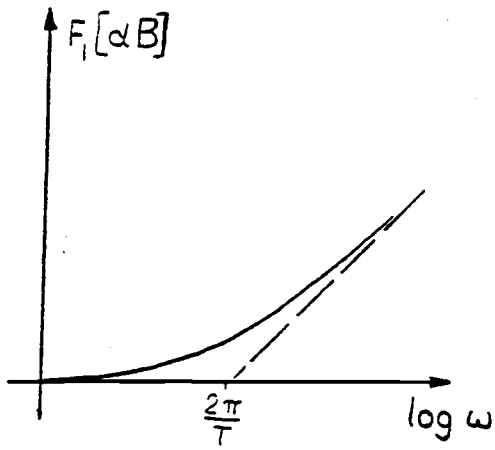

Figure 3.3 Bode-diagram of a first order zero $F_1(s) = 1 + sT$

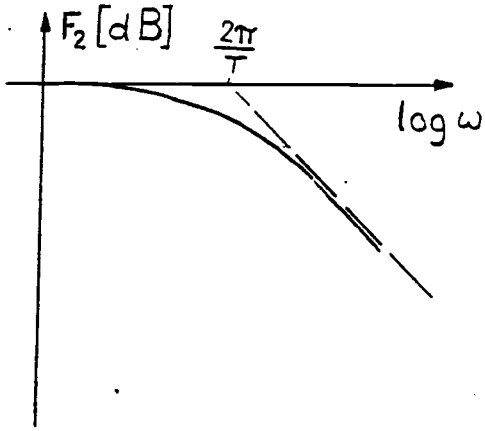

Figure 3.4 Bode-diagram of a first order pole $F_2(s) = 1/(1+sT)$

The slope of the asymptote of $F_1(s)$ is 20dB/decade and that of $F_2(s)$ is -20dB/decade.

Consequently, the following poles, zeros and the factor k from eq.(3.3) are obtained:

poles $p_i = -2\pi \cdot 160\text{Hz}$ $\quad i = 1,\ldots,5$

$p_6 = -2\pi \cdot 3250\text{Hz}$

zeros $z_1 = -2\pi \cdot 60\text{Hz}$ $\quad z_2 = -2\pi \cdot 100\text{Hz}$

$z_3 = -2\pi \cdot 145\text{Hz}$ $\quad z_4 = -2\pi \cdot 150\text{Hz}$

$z_5 = -2\pi \cdot 155\text{Hz}$ $\quad z_6 = -2\pi \cdot 220\text{Hz}$

factor $k = 2.5$

The overall transfer function thus becomes

$$G = G_1 \cdot G_2 \cdot G_3 \quad , \tag{3.4}$$

where

$$G_2 = \frac{1 + a_0 s}{1 + b_0 s}$$

with $a_0 = 7.2343\text{E-}4$ $\quad b_0 = 4.8971\text{E-}5$

and

$$G_3 = \frac{1 + a_1 s + a_2 s^2 + a_3 s^3 + a_4 s^4 + a_5 s^5}{1 + b_1 s + b_2 s^2 + b_3 s^3 + b_4 s^4 + b_5 s^5}$$

with $a_1 = 7.4296\text{E-}3$ $\quad b_1 = 4.9736\text{E-}3$

$a_2 = 2.1122\text{E-}5$ $\quad b_2 = 9.8946\text{E-}6$

$a_3 = 2.8994\text{E-}8$ $\quad b_3 = 9.9424\text{E-}9$

$a_4 = 1.9394\text{E-}11$ $\quad b_4 = 4.8952\text{E-}12$

$a_5 = 5.0485\text{E-}15$ $\quad b_5 = 9.7387\text{E-}16$;

G_1 was determined in eq.(3.3).

Figures 3.5 and 3.6 show the match of the frequency and the impulse responses of the VSG system and the established transfer function G respectively.

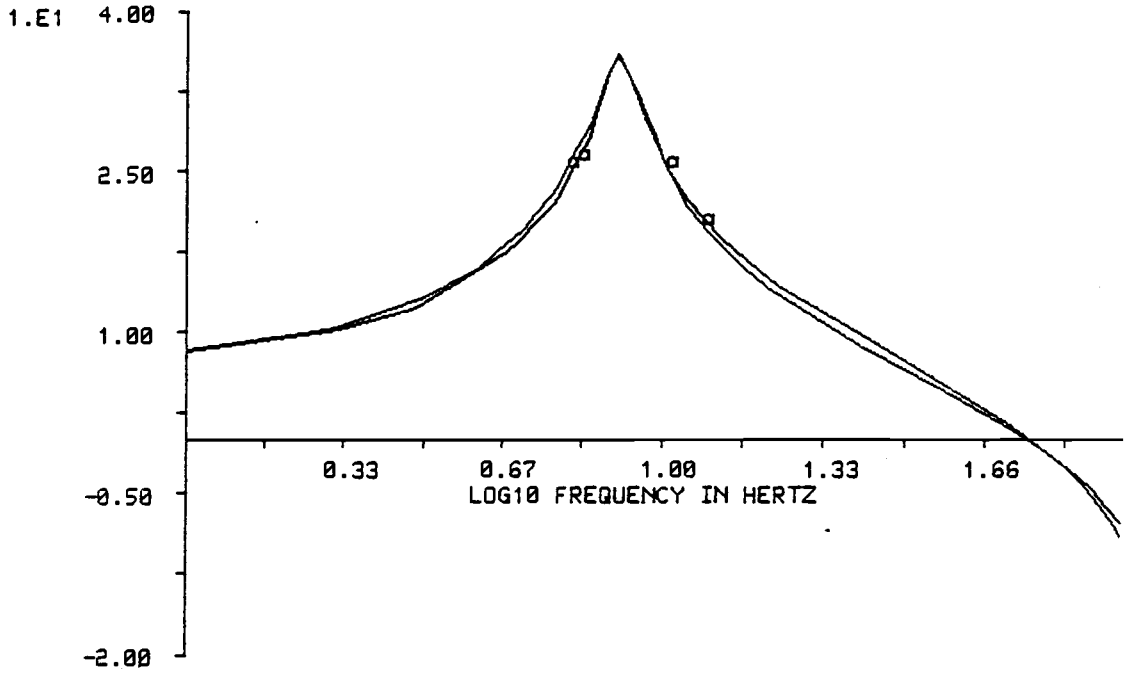

Figure 3.5 Frequency responses of G and the VSG system

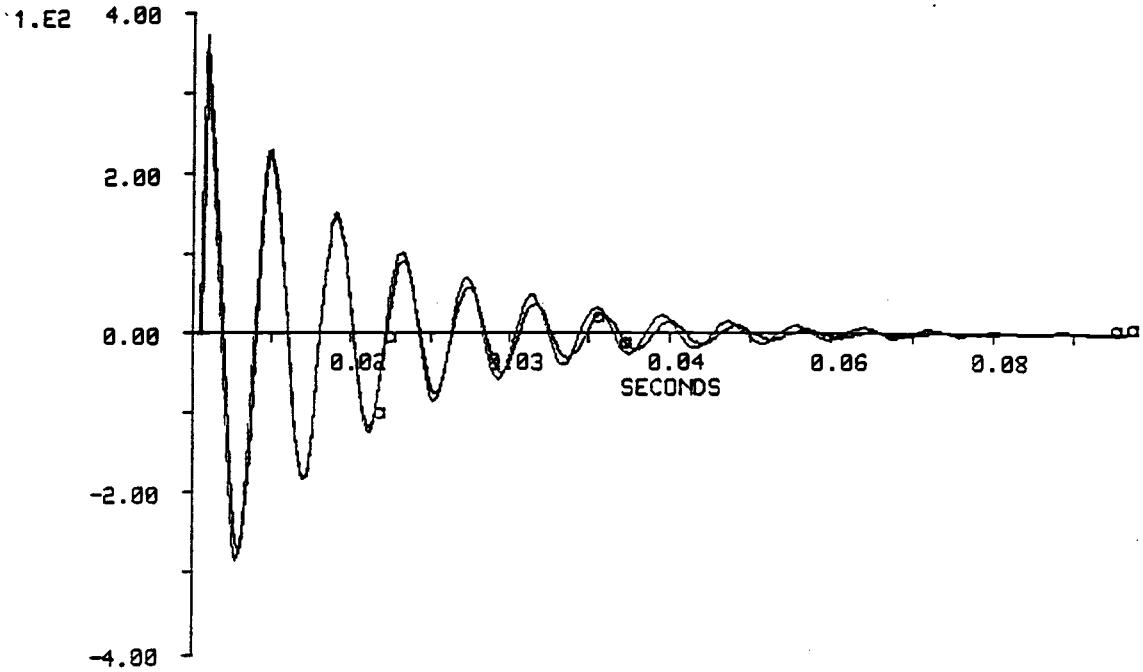

Figure 3.6 Impulse responses of G and the VSG system

III.4 Improvements of the frequency response

III.4.1 Goals

The approximated transfer function G for the frequency response of the VSG system as obtained in section III.3 is not yet satisfactory in two respects:

a) Order of G

The considerations in III.3.2 were based on the overall number of state variables in the entire VSG system. Based on the assumption that the shaft speed ω_m is approximately constant it should be possible to reduce the order of the approximated system.

b) Quality of approximation

Although the VSG system is approximated by a transfer function of the order eight, the deviation of the impulse response of G from the impulse response of the VSG system is still significant.

In the following, two numerical methods are introduced and applied. The first one will give an estimate for the order of the approximated system based on the given sequence of samples from the impulse response of the VSG system. The coefficients of a new transfer function will be the result of the second algorithm, which is however given in the z-domain. The calculation of the coefficients for this new

transfer function makes use of the samples from the step response of both the VSG system and G. The transformation from the z-domain into the s-domain will be performed by a step-invariant transformation.

III.4.2 Numerical determination of the system order

Having available the samples from the impulse response h(0),h(1),..., the system order can be determined by calculating the rank of the Hankel-matrix [6] which is defined as

$$H(m,k) = \begin{bmatrix} h(k) & h(k+1) & \ldots\ldots h(k+m-1) \\ h(k+1) & h(k+2) & \ldots\ldots h(k+m) \\ \vdots & \vdots & \vdots \\ h(k+m-1) & h(k+m) & \ldots\ldots h(k+2m-2) \end{bmatrix} . \qquad (3.5)$$

If m becomes greater than the system order n, the rank of H(m,k)

$$\text{rank}[H(m,k)] = n \quad . \qquad (3.6)$$

The rank of H(m,k) can be determined by calculating the determinant of H(m,k). For $m \geqslant n+1$, this determinant should satisfy

$$\det\,[H(m,k)] = 0 \quad , \qquad (3.7)$$

since the line-vectors are linearly dependent for increasing m while the rank of H(m,k)is constant. In practice however, those determinants will not vanish because the samples from the impulse response are contaminated with noise. Thus, a criterion of significance needs to be introduced. One way to do this is to calculate the average value of the determinant of H(m,k) for each m over all k, and plot the ratio D(m) against m, where

$$D(m) = \frac{|\text{ average value of } \det[H(m,k)]\ |}{|\text{average value of } \det[H(m+1,k)]|} . \qquad (3.8)$$

From this plot, the system order is obtained as the value of m for which D(m) is maximal. As mentioned before, this method is sensitive to noise contamination of the data since it detects similar modes within the impulse response. If the level of noise becomes too high, D(m) may become periodic for varying m. Consequently, the determination of a maximum of D(m) would be complicated. The computation based on the samples of the impulse response of the VSG system yields the following results:

H(2,k) = -0.1044E0	
	D(2) = 0.7037E-2
H(3,k) = -0.1484E2	
	D(3) = 0.5802E-1
H(4,k) = 0.2558E3	
	D(4) = 0.4971E+2
H(5,k) = -0.5147E1	
	D(5) = 0.1371E-2
H(6,k) = -0.3753E4	
	D(6) = 0.1840E+1
H(7,k) = 0.2040E4	
	D(7) = 0.8380E 0
H(8,k) = 0.2434E4	
	D(8) = 0.8481E 0
H(9,k) = 0.2870E4	

The maximum of D(m) is D(4); thus, the numerical determination of the order of the VSG system yields the result

$$n = 4 \ . \tag{3.9}$$

III.4.3 Numerical determination of the transfer function

Considering the discrete time system in Figure 3.7

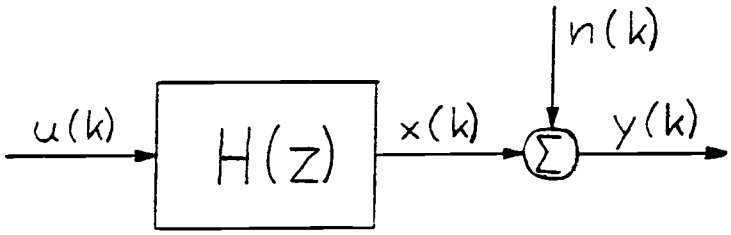

Figure 3.7 Discrete time system

the following input-output description in the time-domain can be obtained [6]:

$$y(k) = \sum_{i=0}^{m} a(i)u(k-i) - \sum_{i=1}^{n} b(i)y(k-i) + v(k) \quad , \tag{3.10}$$

where a(i), b(i) are the coefficients of the numerator and denominator polynomial of H(z) respectively.

v(k) is called output error and is given by

$$v(k) = n(k) + \sum_{i=1}^{n} b(i)n(k-i) \quad . \tag{3.11}$$

Eq. (3.10) may be concatenated to give

$$A(p)\cdot\underline{\Theta} = \underline{y}(p) - \underline{v}(p) \quad , \tag{3.12}$$

where

$$A(p) = \begin{bmatrix} u(k)\ldots\ldots u(k-m) & -y(k-1)\ldots\ldots -y(k-n) \\ u(k+1)\ldots\ldots u(k-m+1) & -y(k) \quad \ldots\ldots -y(k-n+1) \\ \vdots & \vdots \\ u(k+p-1)\ldots u(k+p-m-1) & -y(k+p-2)\ldots -y(k+p-n-1) \end{bmatrix} \tag{3.13}$$

$$\underline{\Theta} = [\ a(0),\ldots,\ a(m),\ b(1),\ldots,\ b(n)] \tag{3.14}$$

$$\underline{y}(p) = [\ y(k),\ldots,\ y(k+p-1)] \tag{3.15}$$

$$\underline{v}(p) = [\ v(1),\ldots,\ v(p)] \quad . \tag{3.16}$$

A matrix Z is assumed to exist which has the same dimension as A(p) and which satisfies the following two conditions

$$E[Z^T v(p)] = 0 \tag{3.17}$$

and

$$E[Z^T A(p)] = Q \quad , \tag{3.18}$$

where Q is a nonsingular matrix.

Multiplication of both sides of eq.(3.12) with Z^T yields

$$Z^T \cdot \underline{y}(p) = Z^T A(p) \cdot \underline{\Theta} + Z^T \cdot \underline{v}(p)$$

or

$$\underline{\Theta}_{iv} = [Z^T A(p)]^{-1} \cdot Z^T \underline{y}(p) \quad , \tag{3.19}$$

where $\underline{\Theta}_{iv}$ is an unbiased and consistent estimate of $\underline{\Theta}$ because of eq.(3.17).

Matrix Z is called the instrumental variable matrix. Its elements are the instrumental variables.

In eq.(3.17) the instrumental variables are observed to be uncorrelated with $\underline{v}(p)$. However, according to eq.(3.18) they are strongly correlated with A(p).

Thus a good choice for Z is given by

$$Z = \begin{bmatrix} u(k) \ldots\ldots u(k-m) & -\bar{x}(k-1) \ldots\ldots -\bar{x}(k-n) \\ u(k+1) \ldots\ldots u(k-m+1) & -\bar{x}(k) \quad \ldots\ldots -\bar{x}(k-n+1) \\ \vdots \qquad\qquad \vdots & \vdots \qquad\qquad \vdots \\ u(k+p-1) \ldots u(k+p-m-1) & -\bar{x}(k+p-2) \ldots -\bar{x}(k+p-n-1) \end{bmatrix}, \tag{3.20}$$

where $\bar{x}(i)$ are the samples of the output of an auxiliary model $\bar{H}(z)$ which is subjected to the same input sequence as H(z). $\bar{H}(z)$ could be any stable transfer function. However, in order to obtain the strong correlation between A(p) and Z^T, the approximated transfer function of the VSG system from eq.(3.4) was chosen for $\bar{H}(z)$.

Figure 3.8 shows the measurement scheme for the determination of $\underline{\Theta}_{iv}$.

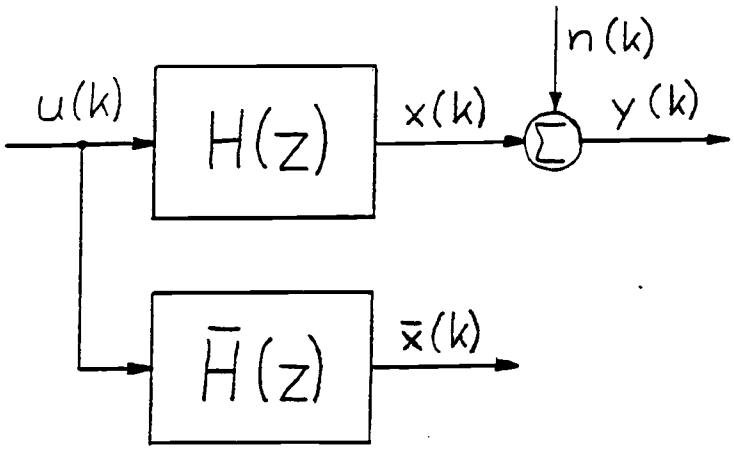

Figure 3.8 Measurement scheme

For the sake of simplicity u(k) was chosen to be a step-function. Assuming that H(z) has the general form

$$H(z) = \frac{a(0) + a(1)z^{-1} + a(2)z^{-2} + a(3)z^{-3} + a(4)z^{-4}}{1.0 + b(1)z^{-1} + b(2)z^{-2} + b(3)z^{-3} + b(4)z^{-4}} \quad (3.21)$$

the computation according to eq.(3.19) yields the coefficients

a(0) = 0.6764E-2	
a(1) = 0.2584E 1	b(1) = -0.2460E 1
a(2) = 0.4100E 0	b(2) = 0.2090E 1
a(3) = -0.2924E 1	b(3) = -0.7909E 0
a(4) = 0.8734E-2	b(4) = 0.1625E 0 .

In order to see if condition (3.17) is satisfied the determinant of Q was calculated as

det[Q] = 0.5453E12 ,

which assures that Q is a nonsingular matrix.

Compliance with condition (3.18) was tested by calculating the trace of $Z^T\underline{v}(p)$. In order to make sure that a desired result is not caused by the trace of either Z^T or $\underline{v}(p)$ being close to zero, condition (3.18) was evaluated from the relation

$$\frac{tr[Z^T\underline{v}(p)]}{tr[Z^T]\cdot tr[\underline{v}(p)]} = 0.1842E-5 \quad , \qquad (3.22)$$

which is considered to be sufficient close to zero.

The poles of H(z) are obtained as

$$z_{1/2} = 0.9957 \pm j0.0513$$

and

$$z_{3/4} = 0.2341 \pm j0.3297 \quad .$$

All poles are within the unit circle of the complex z-plane, thus H(z) is stable.

The final step is to transform H(z) into the continuous time domain. It needs to be mentioned that there can not be a systematic method to perform this transformation. This is due to the fact that all variables in a discrete time system are only defined for discrete instances of time, while variables in the s-domain are defined for all times (although time is assumed to be non-negative in general). However, if the values of the discrete time domain are required to match their corresponding values in the continuous time domain at the sampling points, certain methods for this transformation are available.

For this investigation the step-invariant transformation is chosen, which is based on the assumption that variables in the discrete time domain maintain their values during the sampling interval.

III.4.5 Step-invariant transformation

The transformation of the numerator and denominator polynomial can be performed separately according to the following procedure:

Step 1) Transformation of the denominator

The poles of H(z) were obtained in the previous section. Using the relationship

$$z(i) = \exp[T \cdot s(i)]$$

or

$$s(i) = (1/T) \cdot \ln[z(i)] \quad , \qquad (3.23)$$

where z(i), s(i) denote corresponding points in the z- and s-domain respectively and T the sampling interval, the poles of H(s) are obtained as

$$s_{1/2} = -59.45 \pm j1029.52$$

and

$$s_{3/4} = -18108.9 \pm j19070.2 \quad .$$

Since the poles have negative real parts, stability is preserved by H(s).

Step 2) Transformation of the numerator

The desired H(s) is of the form

$$H(s) = \sum_{k=1}^{n} \frac{A(k)}{s - p(k)} , \tag{3.24}$$

where A(k) are the unknown numerator coefficients

and p(k) are the previously obtained poles.

If H(z) is given by

$$H(z) = \sum_{k=1}^{n} \frac{B(k)}{z - \exp[p(k)\cdot T]} ,$$

the following relation between A(k) and B(k) holds:

$$A(k) = \frac{-B(k)p(k)}{1 - \exp[p(k)\cdot T]} . \tag{3.25}$$

Thus the improved approximated transfer function H(s) of the VSG system is obtained as

$$H(s) = \frac{c(0) + c(1)s + c(2)s^2 + c(3)s^3}{1.0 + d(1)s + d(2)s^2 + d(3)s^3 + d(4)s^4}, \tag{3.26}$$

where

c(0) = 0.85171E 2	d(1) = 0.36337E 5
c(1) = 0.86628E 8	d(2) = 0.69697E 9
c(2) = 0.55206E13	d(3) = 0.12075E12
c(3) = 0.16922E16	d(4) = 0.73549E15 .

Figure 3.9 shows how the impulse responses of the VSG system and H(s) match. Significant improvements compared to Figure 3.5 are visible and were possible while simultaneously reducing the order of the system to one half of the originally assumed order. The conclusion can be made that some state variables of the VSG system have negligible influence on the dynamic behavior of the electrical part of the system. The results also clearly indicate that the conditions mentioned in III.4.1 are not violated.

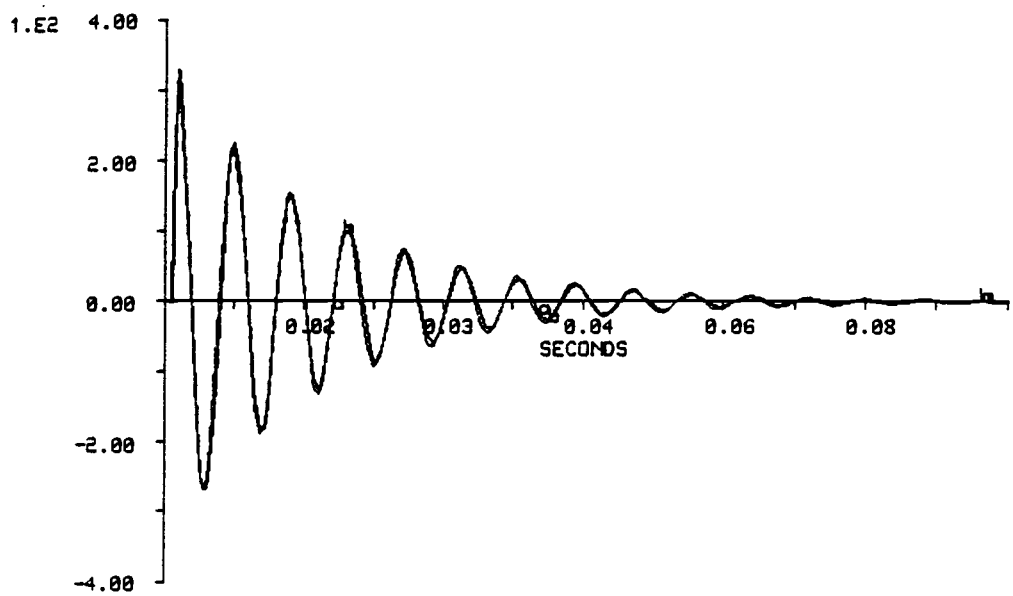

Figure 3.9 Comparison of the impulse responses of H(s) and the VSG system

Chapter IV: DESIGN OF THE FEEDBACK CONTROLLER

IV.1 Introduction

In the previous chapter the linear model of the VSG system was established which was shown to be reducable to a fourth order system without compromising the accuracy of the dynamic response. In this chapter the design of the voltage controller for the VSG system is presented which is based on the transfer function as found in III.4. As already mentioned earlier, it is highly desirable to design a fixed-parameter controller rather than one which needs to be fine-tuned for each change of the operating conditions of the VSG system.

The design will be based on the Root-Locus Method (RLM). The method is applied to a general structure of the control system. The order of the polynomials for the different parts of the controller will be determined through the application of a criterion which will lead to a sub-optimal performance of the controller.

IV.2 The Root-Locus-Method as tool for design

The dynamic behavior of a closed-loop control system is determined by the location of its poles in the complex s-plane, i.e. for a closed-loop system with the forward transfer function G(s) and feedback transfer function H(s) the closed-loop transfer function $G_C(s)$ is obtained as

$$G_C(s) = \frac{G(s)}{1 + G(s)H(s)} \quad . \tag{4.1}$$

The poles of G_C are determined by the roots of the characteristic equation

$$1 + G(s)H(s) = 0 \tag{4.2}$$

For the design of the controller it is important to trace the locations (loci) of the roots if G(s) is multiplied with a variable amplification factor k. In particular the knowledge of the root loci for k = 0 and for k approaching infinity is important. The characteristic equation including k becomes

$$G(s)H(s) = - \frac{1}{k} \quad . \tag{4.3}$$

For k approaching zero G(s)H(s) goes to infinity, which is only possible if the roots of eq.(4.3) coincide with the poles of the open-loop transfer function G(s)H(s).

For k approaching infinity, G(s)H(s) goes to zero. Therefore, the roots of eq.(4.3) coincide with the zeros of the open-loop transfer function.

In closed-loop control systems usually the number of poles exceeds the number of zeros of the open-loop transfer function. Consequently, for k approaching infinity there are poles which can not coincide with zeros of the open-loop transfer function since only one pole can coincide with one zero. It is found that the remaining poles move towards infinity along well defined asymptotes. These asymptotes have the following properties:

i) their number is determined by the difference between the number of poles n and the number of zeros q of G_C.

ii) due to the symmetry of the problem with respect to the real axis all asymptotes meet in one point on the real axis which is called the "center of gravity (CG)". Its coordinate is determined by

$$\sigma_{CG} = \frac{\sum_i \text{poles} - \sum_j \text{zeros}}{n - q} \quad . \tag{4.4}$$

iii) the angle under which an asymptote meets the real axis is determined by the equation

$$\measuredangle = \frac{\pi - \nu \cdot 2\pi}{n - q} \quad [\text{rad}] \qquad (4.5)$$

with $\nu = 0, 1, \ldots, n-q-1$,

i.e. if there is one more pole than zeros the pole moves towards infinity along the negative real axis; or if the number of poles exceeds the number of zeros by two, the two remaining poles go to infinity along two asymptotes which are orthogonal to the real axis, and so on.

This knowledge about the behavior of the roots of a closed-loop system can be used to predict the dynamic behavior of a system depending on its closed-loop amplification. In addition, the exact trace (root-locus) of the roots depending on the changing value of k can be obtained if the possibility is given to quickly calculate the roots of higher order polynomials. A powerful guidance to a proper design of the controller is given by the two properties of the RLM as was explained earlier, namely:

a) For an infinite small value of the closed-loop amplification k the roots of G_C coincide with the poles of the open-loop transfer function

b) For an infinite large value of k the roots of G_C either approach the zeros of the open-loop transfer function or move towards infinity along the asymptotes.

IV.3 Structure of the feedback controller

The desired structure of the feedback controller is given in Figure 4.1

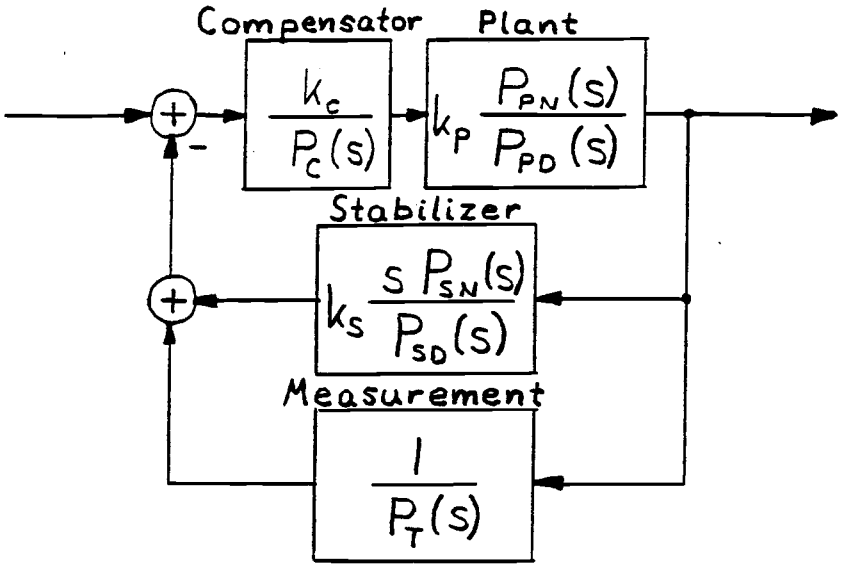

Figure 4.1 Structure of the control system

The idea behind this structure is the following:

a) The measurement branch feeds back the output signal with some small delay as determined by $P_T(s)$.

b) The stabilizer branch reacts on changes of the output signal. Depending on the speed of change and the sign of its amplification, the stabilizer output either adds to or diminishes the measurement signal in order to stabilize the output signal of the system.

c) The compensator has to enforce a zero steady state error between input and output signal.

Let all polynomials P_i, for i = C,T,PN,PD,SN,SD, satisfy:

$$P_i(s=0) = 1 \quad . \tag{4.6}$$

From Figure 4.1 the following transfer functions are obtained:

a) The forward-loop transfer function

$$G = k_C k_P \frac{P_{PN}(s)}{P_C(s)P_{PD}(s)} \quad , \tag{4.7}$$

b) the feedback-loop transfer function

$$H = k_S \frac{sP_{SN}(s)}{P_{SD}(s)} + \frac{1}{P_T(s)} = \frac{k_S sP_{SN}P_T + P_{SD}}{P_{SD}P_T} \quad , \tag{4.8}$$

c) the open-loop transfer function

$$GH = k_C k_P \frac{k_S sP_{SN}P_T P_{PN} + P_{SD}P_{PN}}{P_C P_{PD} P_{SD} P_T} \quad . \tag{4.9}$$

Let α, β and γ be defined as the orders of the following polynomials, where $[P_i]$ denotes the order of the polynomial P_i:

$$\alpha = [k_S sP_{SN}P_T] \quad , \tag{4.10}$$

$$\beta = [P_{SD}P_{PN}] \tag{4.11}$$

and

$$\gamma = [P_C P_{PD} P_{SD} P_T] . \tag{4.12}$$

In the following, relations between the orders of the polynomials P_C , P_T , P_{SN} and P_{SD} are derived such that the root-locus of the closed-loop system has a desirable number of asymptotes.

The loci of the zeros of the open-loop transfer function are given by

$$P_{PN} = 0 \quad \text{(zeros of the plant)} \tag{4.13}$$

and

$$k_S s P_{SN} P_T + P_{SD} = 0 \quad . \tag{4.14}$$

In the closed-loop system these loci constitute the loci of the roots for k_C approaching infinity. The zeros of the plant are given. However, the stabilizer polynomials P_{SD} and P_{SN} can be chosen such that additional zeros are placed at locations which would yield a desirable root locus of the closed-loop system.

The root-locus of a closed-loop system is called "desirable" if the following conditions are satisfied:

a) Unstable operation can be prevented even if the gain of the forward loop transfer function approaches infinity.

b) Improvements of the system response with respect to the speed of response and overshoot can be easily made without causing conflicting requirements for the parameters of the controller.

In the following the orders of all polynomials in the closed-loop system are determined.

P_T represents the delay of the measurement device and is assumed to be of first order

$$P_T = 1 + sT_m \,. \tag{4.15}$$

A pure integrator is chosen for the compensator in order to enforce zero steady-state error between input and output. P_{PN} and P_{PD} are the numerator and denominator polynomials of the linear model of the VSG system as derived in III.4. The order of the following polynomials is already determined:

$$[P_{PN}] = 3 \quad , \tag{4.16}$$

$$[P_{PD}] = 4 \quad , \tag{4.17}$$

$$[P_C] = 1 \quad , \tag{4.18}$$

and

$$[P_T] = 1 \quad . \tag{4.19}$$

This gives the following relations for α, β and γ:

$$\alpha = [P_{SN}] + 5 \quad , \tag{4.20}$$

$$\beta = [P_{SD}] + 3 \quad , \tag{4.21}$$

$$\gamma = [P_{SD}] + 6 \quad . \tag{4.22}$$

A decision for the desired number of asymptotes of G_C has to be made at this point. A number of asymptotes larger than two is undesirable because then asymptotes of G_C reach in the right half-plane of the s-domain and poles move in this half-plane along those asymptotes.

The choice was made for a design with one asymptote because it is expected that the range of k_C, for which G_C has unstable poles, is smaller than for a design with two asymptotes. This requires that

$$\gamma - \alpha = 1 \quad . \tag{4.23}$$

Consequently

$$[P_{SD}] = [P_{SN}] \tag{4.24}$$

which yields

$$\alpha - \beta = 2 \quad . \tag{4.25}$$

In order to achieve maximum reliability of the controller it is desirable to design the controller as simple as possible. Therefore the choice is made for

$$[P_{SD}] = [P_{SN}] = 1 \tag{4.26}$$

which results in

$$P_{SD} = 1 + sT_{SD} \tag{4.27}$$

and

$$P_{SN} = 1 + sT_{SN} . \tag{4.28}$$

The orders of all polynomials in the closed-loop system have now been determined.

IV.4 Determination of the parameters

The freedom of design is now limited to the proper choice of the parameters T_{SD}, T_{SN}, k_S and k_C.
T_m, the time constant of the measurement delay is assumed to be

$$T_m = 0.1 \text{ msec} . \tag{4.29}$$

The plant poles are located at

$$s_{1/2} = -50.45 \pm j1029.52$$

and

$$s_{3/4} = -18108.9 \pm j19070.2 ,$$

as found in III.4.

The first pole pair are the dominant poles which need to be removed from the imaginary axis as far as possible. This can be achieved by placing zeros of the open-loop transfer function GH to the left of those poles. The zeros of GH are given by eq.(4.13) and eq.(4.14).
The zeros of the linear model are

$$z_1 = -308.034 ,$$

$$z_2 = -67984.9$$

and $$z_3 = -949127.0 .$$

By choosing the parameters T_{SD}, T_{SN} and k_S the remaining zeros given by eq.(4.14) can be placed. This choice can be made using again the RLM.

Considering eq.(4.14) as the characteristic equation of the following system

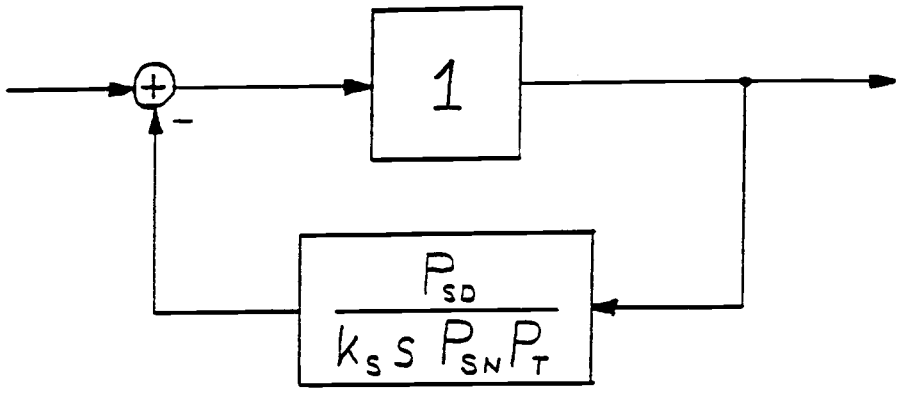

Figure 4.2 Closed-loop model representing eq.(4.14)

the root-locus of these zeros depending on the choice of k_S, T_{SD} and T_{SN} can be observed. In addition, the observation can be made that if these zeros are placed too far away from the dominant poles of G , k_C has to be chosen large in order to remove the dominant poles from the imaginary axis. This causes at the same time the other complex conjugate pole pair of G to move too far to the right towards the imaginary axis.

As a compromise between the contradicting desires to remove the dominant poles from the imaginary axis as far as possible, and at the same time not bringing the other complex conjugate pole pair too far to the right by choosing k_C large, the following values for k_S, T_{SD} and T_{SN} were found:

$$T_{SN} = 0.1E-2 \quad , \tag{4.30}$$

$$T_{S0} = 0.2222E-3 \quad , \tag{4.31}$$

and

$$k_S = 0.32E-2 \quad . \tag{4.32}$$

This choice of the parameters gives the following roots of eq.(4.14) :

$$r_{1/2} = -521.45 \pm j211.06 \quad ,$$

and

$$r_3 = -9955.8 \quad .$$

Figure 4.3 and Figure 4.4 show the root-locus of the closed-loop system. Figure 4.4 shows the region around the origin of Figure 4.3 enlarged.

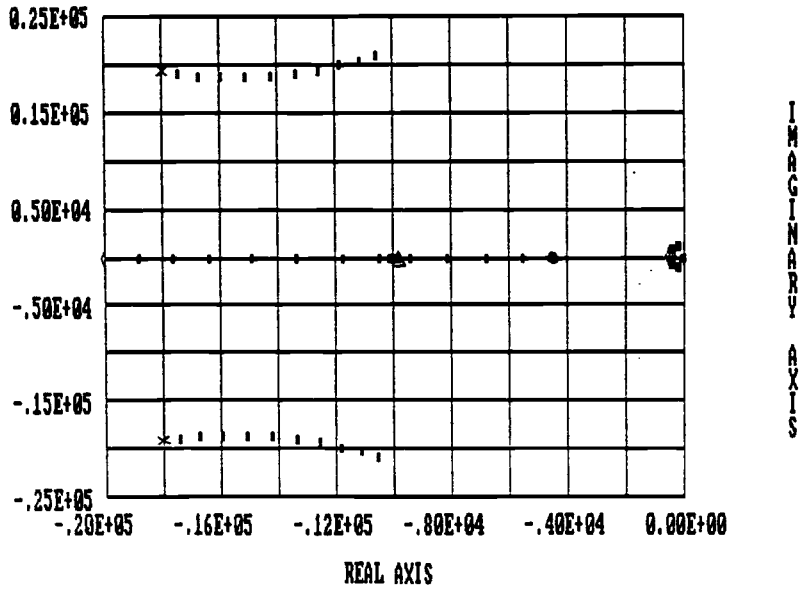

Figure 4.3 Root-Locus of the closed-loop system

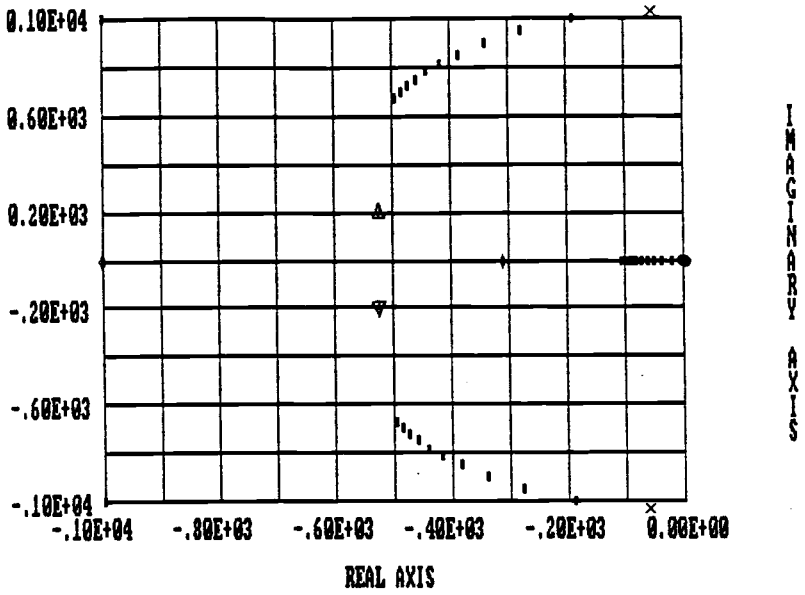

Figure 4.4 Region around the origin of Figure 4.3 enlarged

The convention for the symbols is as follows:

× denote plant poles,

• denote poles of GH created by P_C, P_{SD} and P_T,

ΔV denote zeros of GH created by choice of T_{SD}, T_{SN}, and k_C,

◊ denote plant zeros,

▮ trace of root-locus of the closed-loop system.

From Figure 4.3 the following results for increasing k_c are obtained:

i) Both poles created by P_{SD} and P_T move to zeros on their left.

ii) The plant poles far out in the left half-plane of the s-domain move towards the imaginary axis. Therefore, while increasing k_c the root-locus of those two poles has to be observed carefully because they move towards the right half-plane of the s-domain and can destroy the stability of the system.

In Figure 4.4 the following observations are made for increasing k_c:

i) The dominant poles of the plant move towards the zeros created by eq.(4.14). This is desirable.

ii) The pole in the origin created by P_c moves slowly towards one of the plant zeros. This pole close to the imaginary axis has to be accepted because the plant zero is fixed and the locus of the pole is given by the general structure of the closed-loop system.

The best choice of k_c has to be made during simulations of the complete VSG system including the just designed voltage controller.

Chapter V: VERIFICATION OF THE CONTROLLER'S EFFECTIVENESS

V.1 Introduction

The result of the investigation in chapter IV is the complete design of the voltage controller for the VSG system. The voltage controller is designed as simple as possible and is easy to implement due to the fact that it contains only one differentiator.

However, the effectiveness of the controller over the entire range of operation of the VSG system still needs to be proven. The implementation will be performed step by step. First the controller will be implemented as controller for the linear model derived in section III.4 and then as controller for the simplified system from which this linear model was derived. As the most important step of this chapter the effectiveness of the controller will be shown as it is implemented in the VSG system. Limitations in the stable range of operation will be investigated. Finally the performance of the VSG system with the voltage controller as designed here will be compared with the step response of the VSG system having implemented a controller which is based on a conventional design.

V.2 Dynamic behavior of the closed-loop system (linear model and simplified system)

Figures 5.1, 5.2 and 5.3 show the step responses of the closed-loop model of the system for increasing k_c.

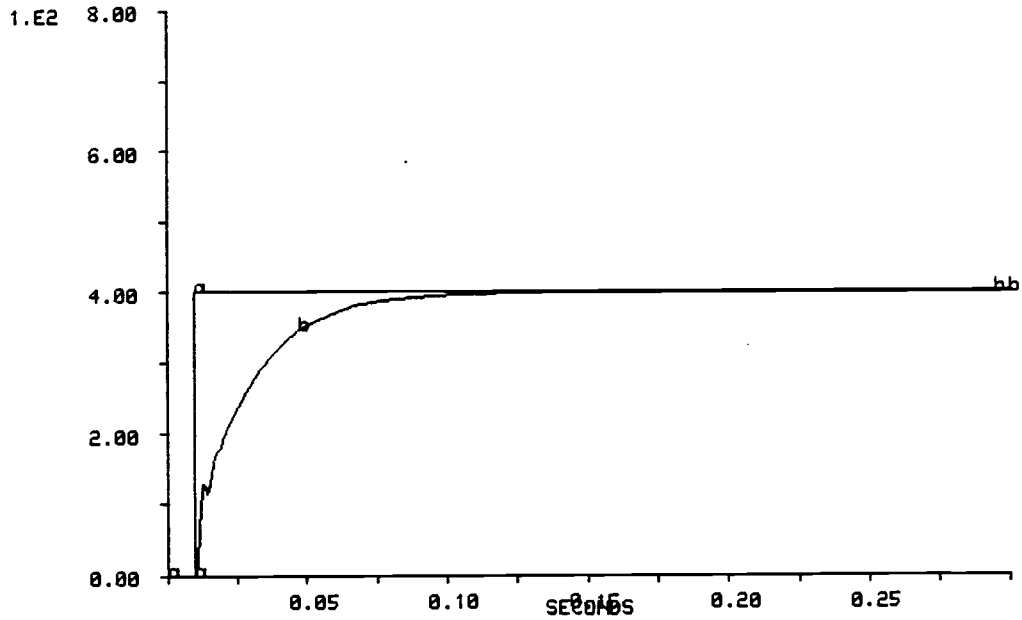

Figure 5.1 Step response of the closed-loop system (k_c = 50.0)

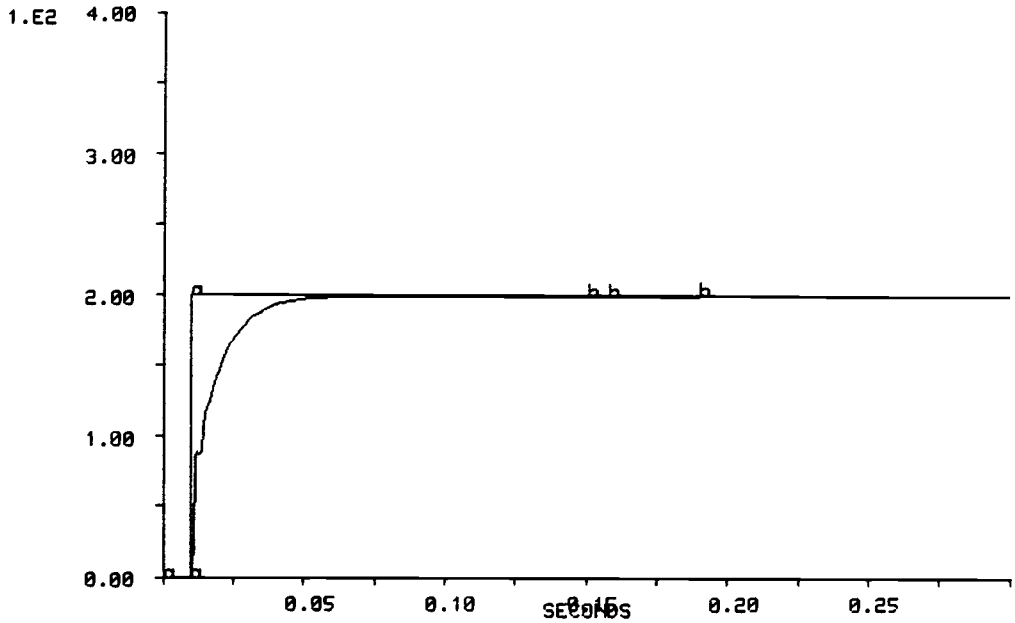

Figure 5.2 Step response of the closed-loop system

(k_c = 100.0)

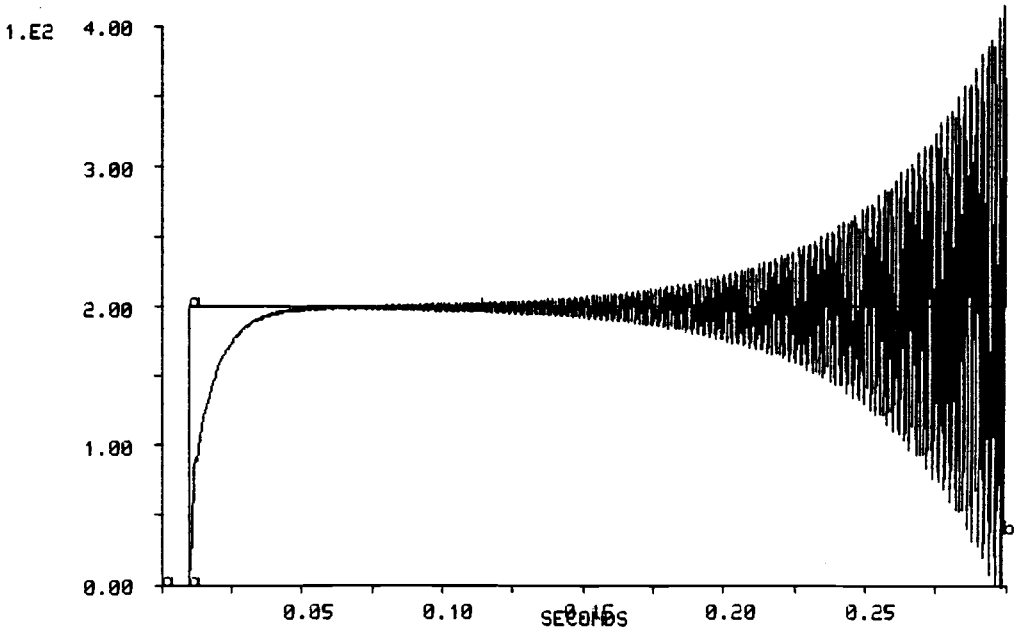

Figure 5.3 Step response of the closed-loop system

(k_c = 122.0)

Two observations can be made which confirm the expectations from chapter IV.4:

i) As long as the complex conjugate pole pair of the model H(s) far out in the left half-plane s-plane does not move into the right half-plane caused by increasing k_c over k_c = 120.0, an improvement in the speed of response of the closed-loop system can be observed for increasing k_c as shown in Figures 5.1 and 5.2. This improvement is due to the fact that the designed controller causes the dominant complex conjugate pole pair of H(s) to move away from the imaginary axis and into the left half-plane as seen in Figure 4.4.

ii) Increasing k_c beyond a certain value (+120.0) causes the conjugate complex pole pair far out in the left half-plane to move into the right half-plane and the system becomes unstable as shown in Figure 5.3 .

The controller is implemented to the simplified version of the VSG system from which the linear model was derived in chapter III. Figures 5.4 and 5.5 show the step responses for k_c = 40.0. The system is operating at 0.1% slip and steps of 5% and 30% are applied to the terminal voltage respectively.

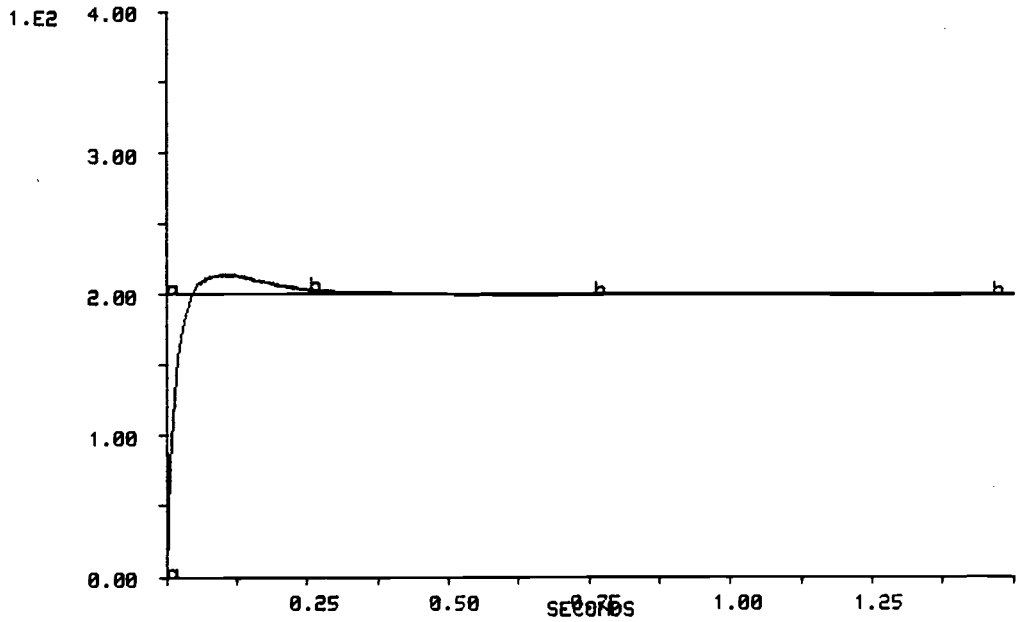

Figure 5.4 Step response of the simplified VSG system

(Δu = 5%)

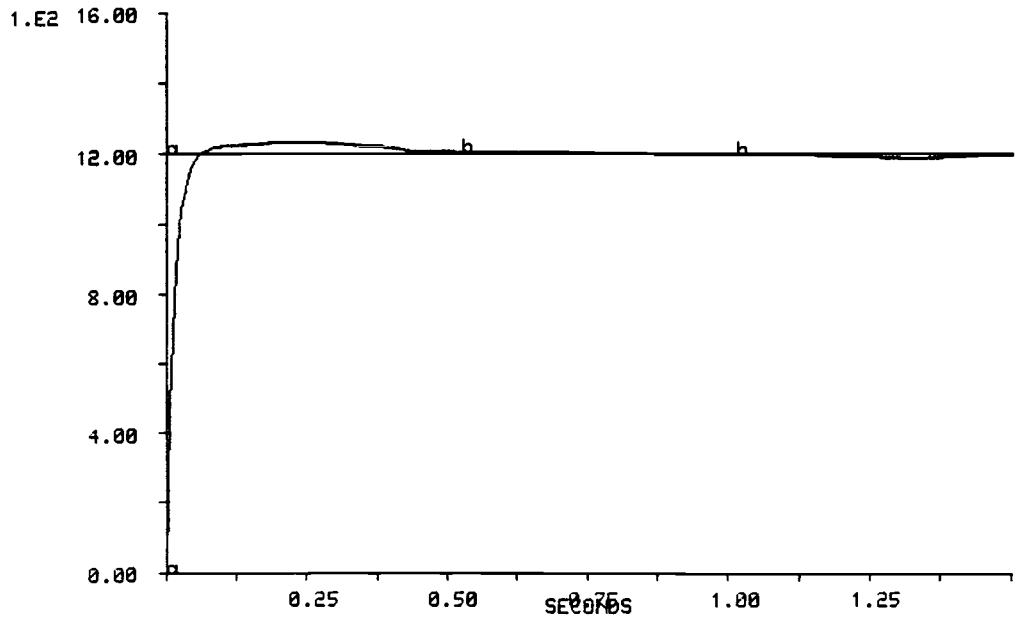

Figure 5.5 Step response of the simplified VSG system

(Δu = 30%)

Compared to the step responses of the closed-loop model in Figures 5.1 and 5.2 an overshoot in the step response is observed in Figures 5.4 and 5.5. Comparing the shape of the responses in Figure 5.4 and Figure 5.5 the non-linear behavior of the system becomes obvious. The input signals differ only in their amplitude. However, the output signals differ in their percentage overshoots as well as their settling times. It is worthwhile to mention that the system is able to follow steps of up to 30% in V_{ll}^{S} without going unstable.

V.3 Dynamic behavior of the VSG system including the voltage controller

Figures 5.6 through 5.10 show the step responses of the complete VSG system including the voltage controller. Results of the system operating at slip values of 0.1%, 20%, 40%, 60% and 80% are shown. The relative step amplitude in V_{ll}^{S} is 5%, the closed-loop amplification is $k_c = 40.0$.

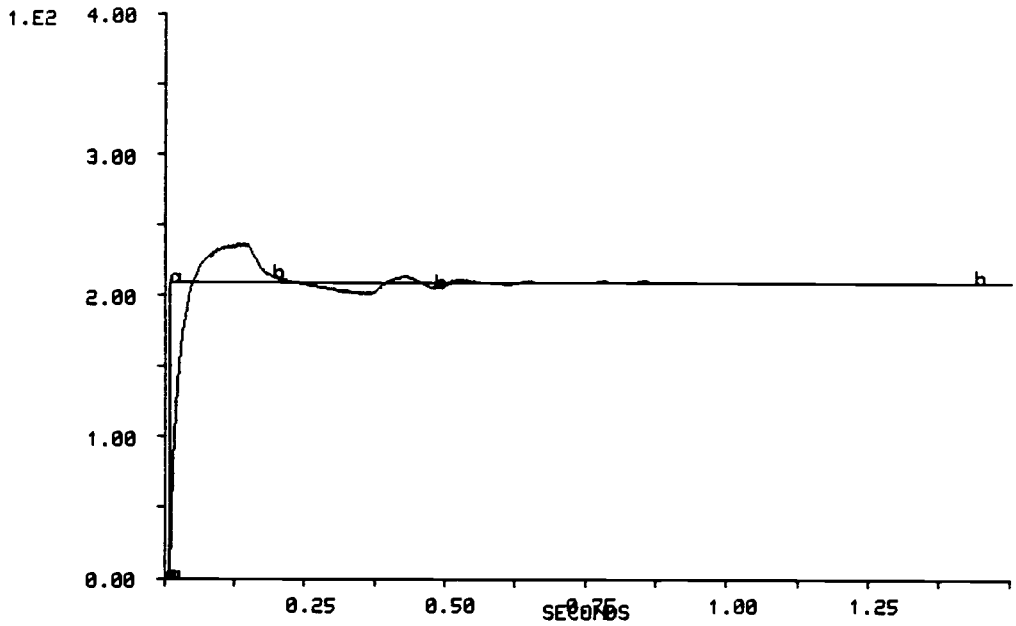

Figure 5.6 Step response of the VSG system (0.1% slip)

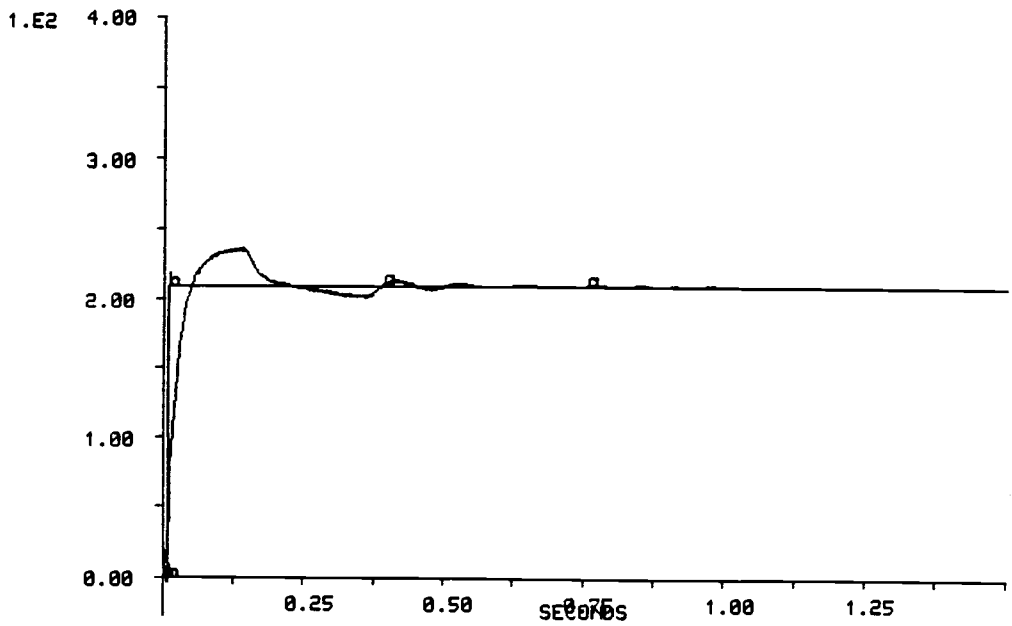

Figure 5.7 Step response of the VSG system (20.0% slip)

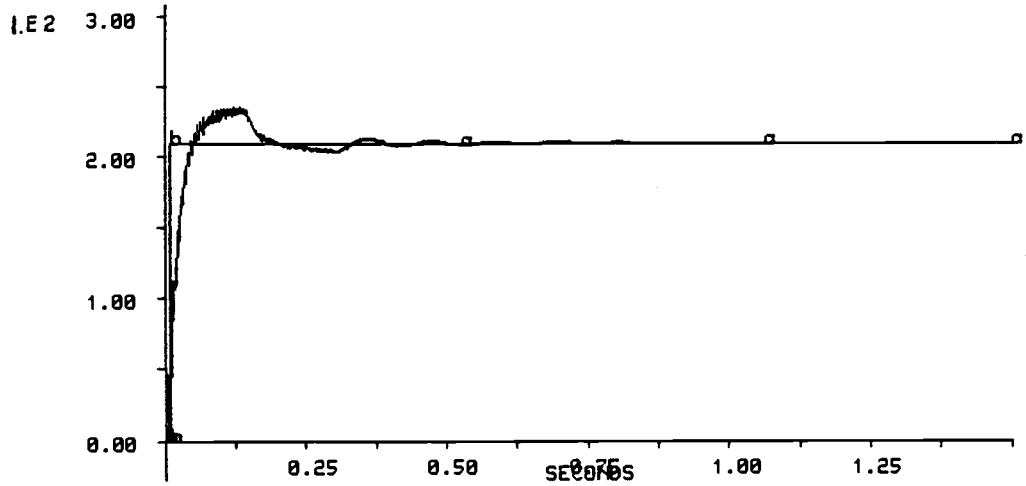

Figure 5.8 Step response of the VSG system (40.0% slip)

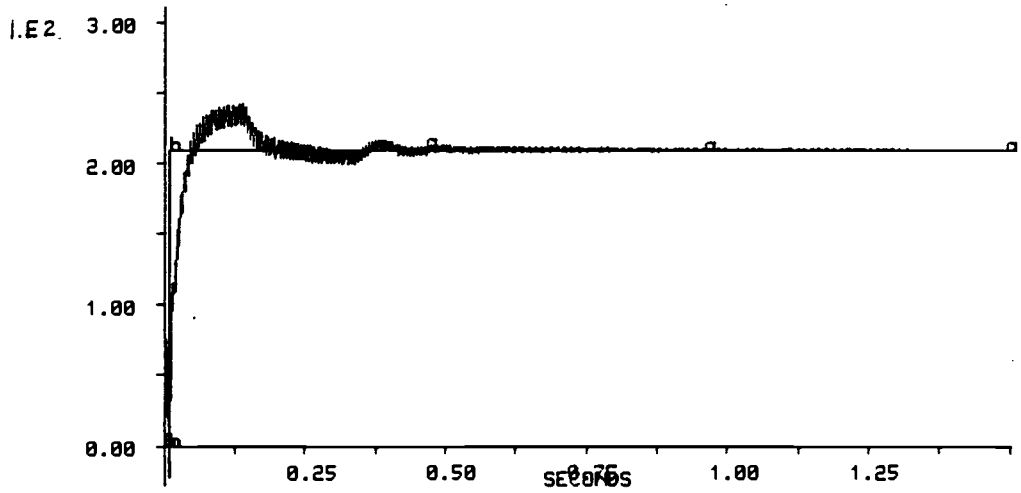

Figure 5.9 Step response of the VSG system (60.0% slip)

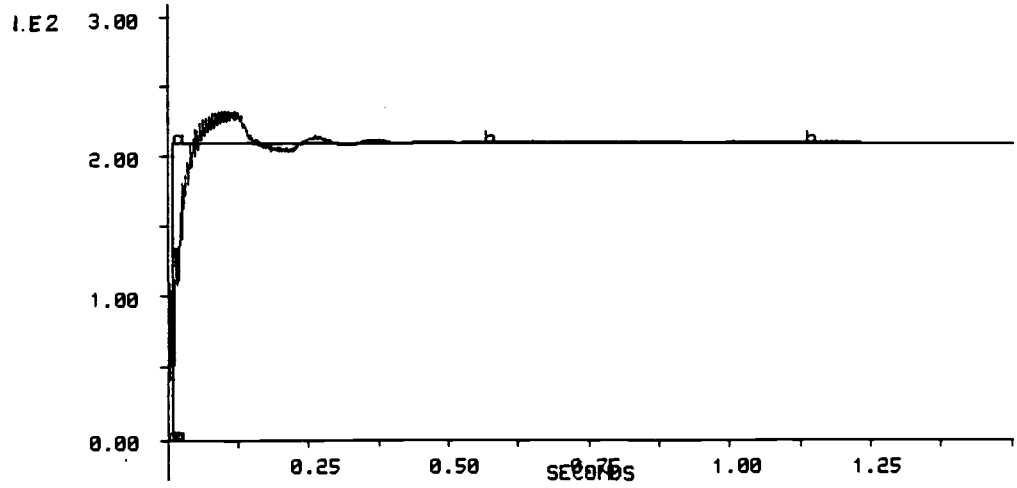

Figure 5.10 Step response of the VSG system (80.0% slip)

Two observations can be made:

i) The settling time and the percentage overshoot in the step responses decrease for increasing slips and

ii) for increasing slips the tendency of the voltage to oscillate with a high frequency increases.

The first observation shows that the point of operation with 0.1% slip is the most critical in terms of stability. This proves that the right choice for the most critical mode of operation was made in section III.3.1.

The second observation shows a phenomenon which could not have been discovered in the investigation of the frequency responses in section III.3, since only the amplitudes of frequencies up to 2kHz were calculated. However, in section III.4 the observation was made that there exists a second conjugate complex pole pair at about 18kHz which is well damped for 0.1% slip. A further investigation would have been necessary in order to find the loci of those roots for higher slips.

Simulations at higher slips show that the system becomes unstable if for constant k_c the amplitude of the steps in V_{α}^{s} is increased or if for constant step-amplitude k_c is increased. It is suspected that for higher slips this second pole pair is either located closer at the imaginary axis or moving faster towards the imaginary axis for increasing k_c.

Comparing the results from the implementation of the controller in the VSG system with those results obtained from the implementation in the simplified system (Figures 5.4 and 5.5), an increase in the settling time can be observed for the step responses of the VSG system. This is due to the influence of the dynamics of the mechanical system caused by changes in ω_m. Table 5.1 shows the settling times t_s (V_{ll}^s within 5% of its final value) for increasing slip s_o;k_c = 40.0 and a 5% step in V_{ll}^s is applied.

s_o[%]	t_s[sec]
0.1	0.36
20.0	0.34
40.0	0.17
60.0	0.16
80.0	0.14

Table 5.1 Settling times for increasing slip

The conclusion is made that the VSG system is able to follow controlled steps in V_{ll}^s of up to 5% while operating at any slip and k_c being constant.

A first step towards the design of a simple adaptive controller was made in order to allow steps of up to 20% in V_{ll}^s over the entire range of operation, varying only the closed-loop amplification k_c. Figures 5.11 through 5.15 show the step responses of the VSG system for a step of 20% in V_{ll}^s and decreasing k_c, $k_c = f(s_o)$.

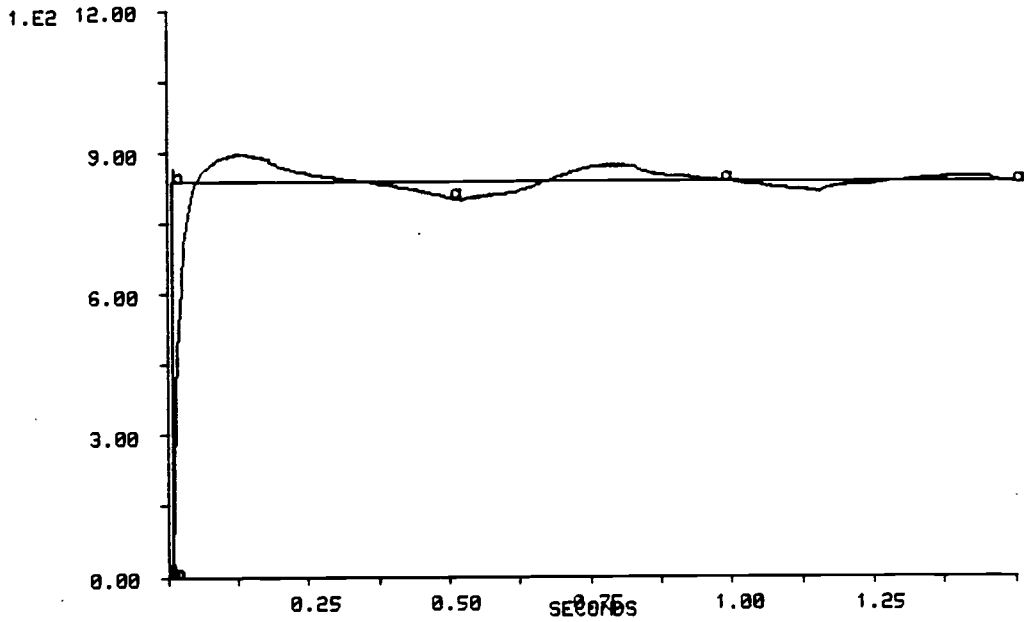

Figure 5.11 Step response of the VSG system

(k_C = 50 and s_o = 0.1%)

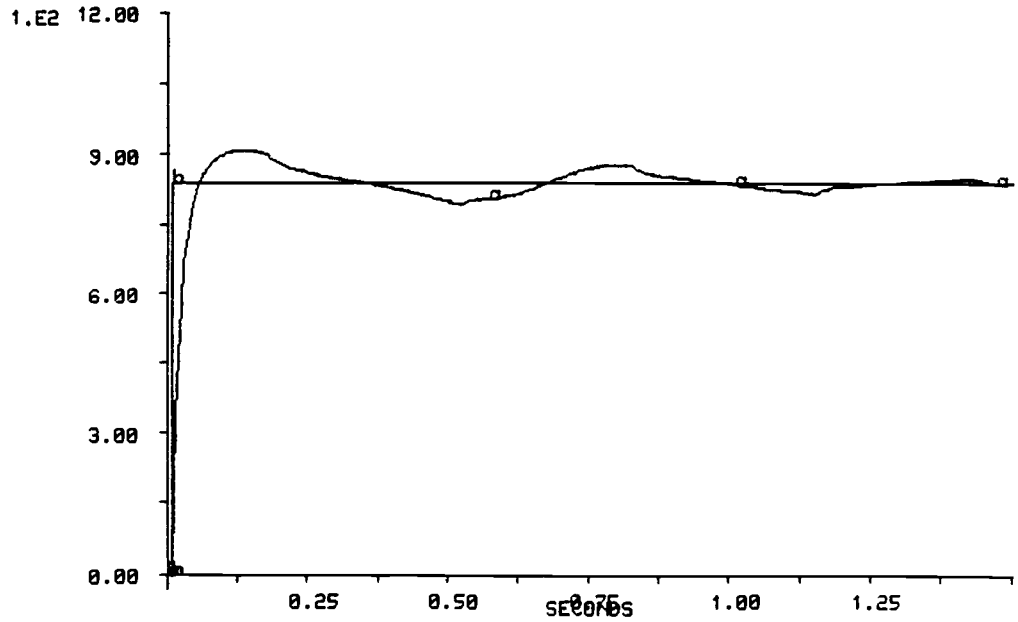

Figure 5.12 Same as Fig. 5.11, but k_C = 40 and s_o = 20%

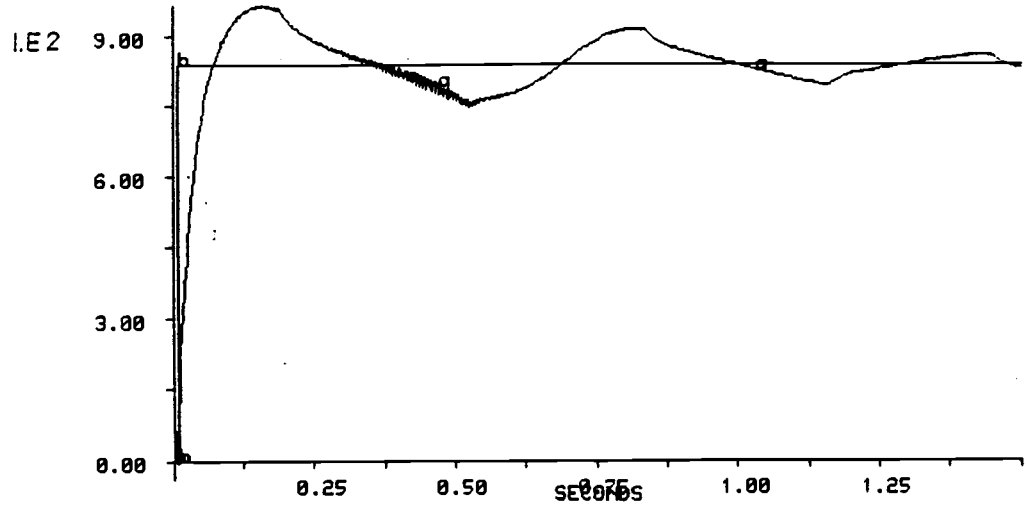

Figure 5.13 Same as Fig. 5.11, but k_c = 20 and s_o = 40%

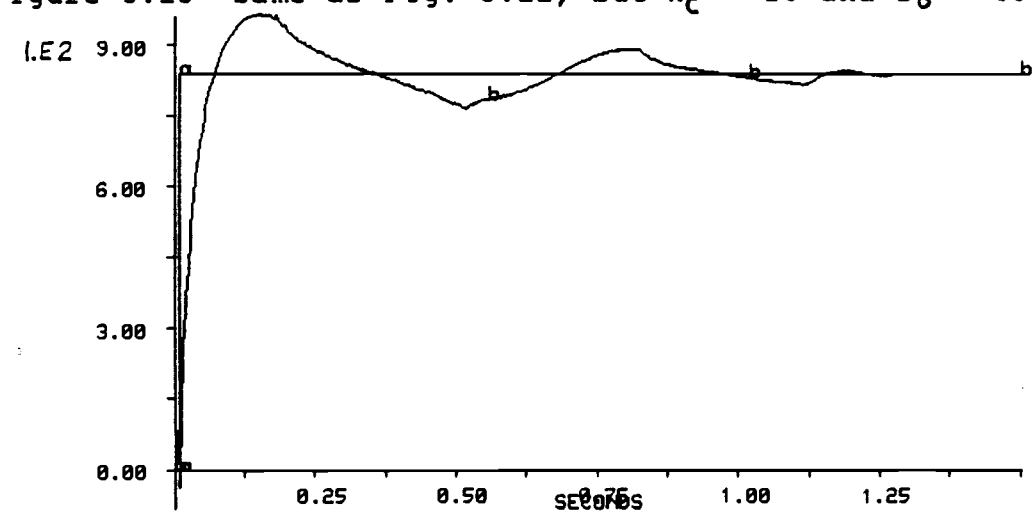

Figure 5.14 Same as Fig. 5.11, but k_c = 20 and s_o = 60%

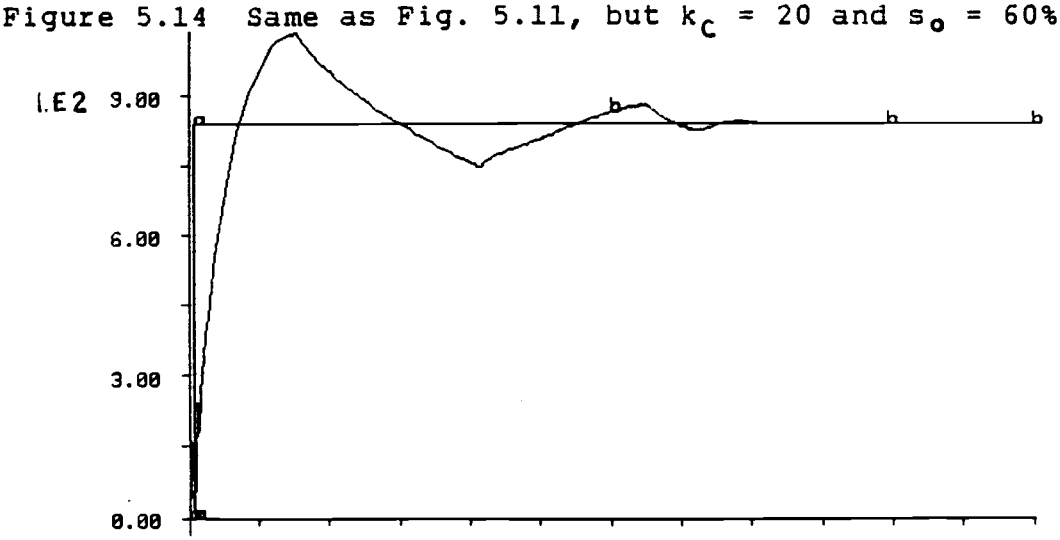

Figure 5.15 Same as Fig. 5.11, but k_c = 10 and s_o = 80%

Table 5.2 shows the settling times t_s (V_{ll}^s within 5% of its final value) for increasing slip s_o and decreasing k_c .

s_o[%]	k_c[ ]	t_s[sec]
0.1	50.0	0.52
20.0	40.0	0.55
40.0	20.0	0.87
60.0	20.0	0.85
80.0	10.0	0.60

Table 5.2 settling times t_s for increasing slips s_o and decreasing k_c

The result shows that higher steps in V_{ll}^s are possible if k_c is chosen smaller, i.e. if k_c is chosen constant to k_c = 10 then steps of up to 20% in V_{ll}^s are possible over the entire range of operation at the cost of increased settling times.

V.4 Comparison with a conventional controller design

Figure 5.16 shows the block diagram for this conventional controller design. This design is based on the controller structure employed by conventional generators which generally are of the synchronous type.

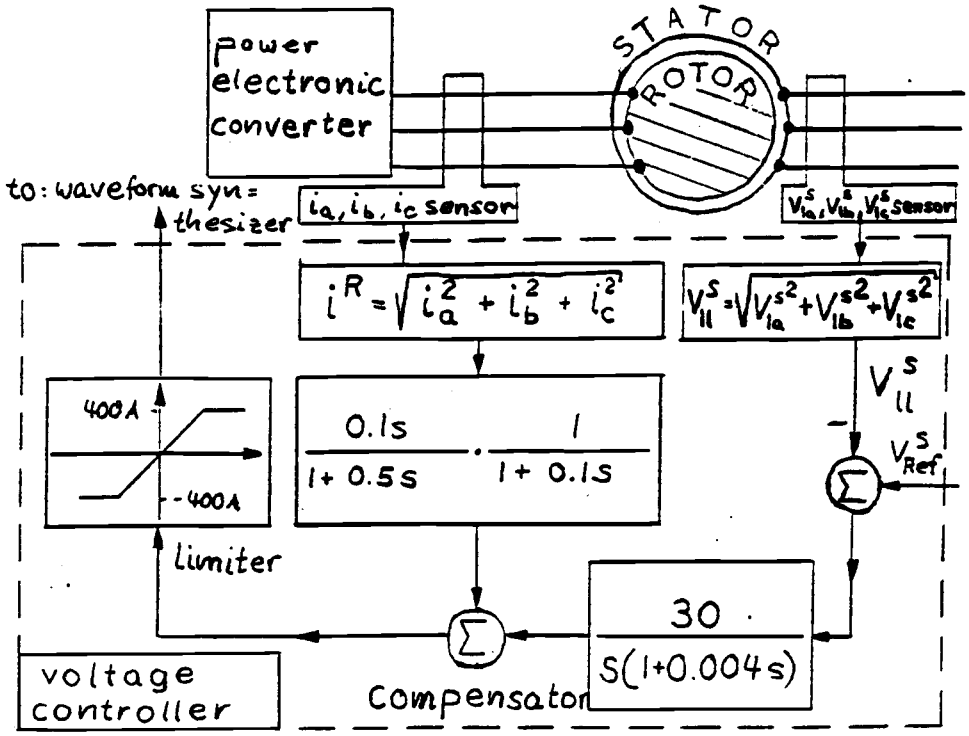

Figure 5.16 Block diagram of a conventional controller design

In contrast to this controller structure Figure 5.17 shows the structure of the controller as it was designed in this thesis. The important improvement of this new design is the fact that the measurement of the rotor currents is no longer required.

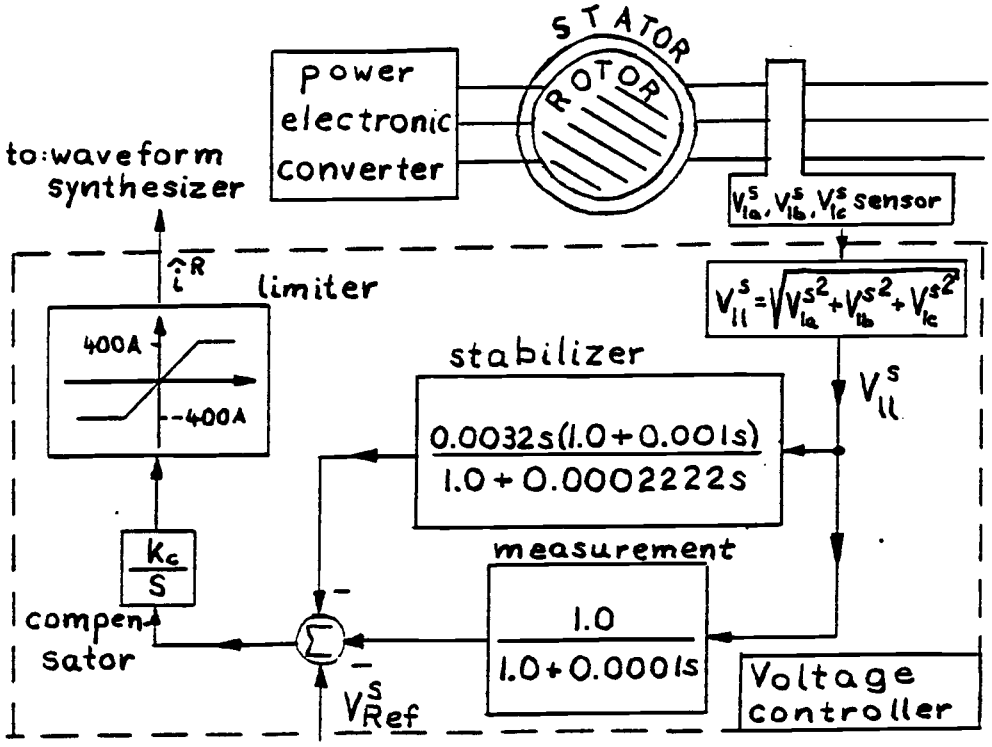

Figure 5.17 Block diagram of the new controller design

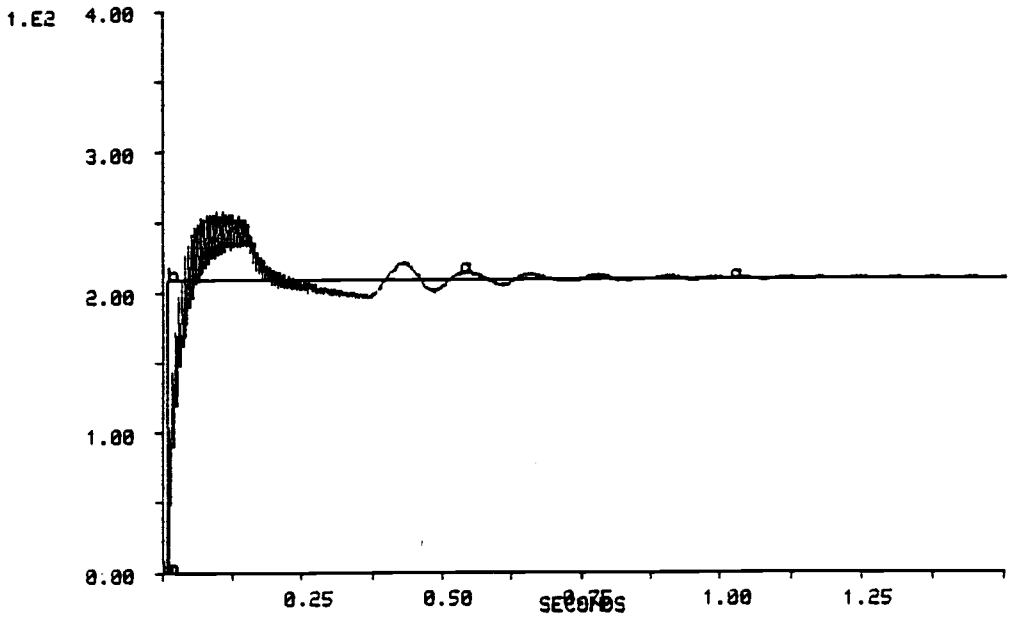

Figure 5.18 Step response of the VSG system with a conventional controller design

Figure 5.18 shows the step response of the VSG system for a 5% step in V_{ll}^{S} and a slip of 0.1% with the controller based on this conventional design.

Comparing this step response with the step response of the VSG system in Figure 5.6, the drawbacks of this conventional design are clearly visible:

i) The settling time (V_{ll}^{S} within 5% of its final value) is considerably higher (0.45sec),

ii) the percentage overshoot is higher and

iii) the high frequency oscillation in V_{ll}^{S} is already present at small slips.

Moreover, the highest ampltude of a step change to V_{ll}^{S} which does not cause the VSG system to become unstable, is significantly lower for the conventional controller than for the controller as proposed in this thesis.

Chapter VI: CONCLUSIONS

The goal of this investigation was the design of a non-complex but effective controller for the VSG system. The resulting controller did not only satisfy these requirements but also proved to be effective over the entire range of operation of the VSG system. By using the terminal voltage of the doubly-excited machine as the controller's input, the required input information is reduced to an absolute minimum. Constraints with respect to the practical implementation are also met due to the fact that the controller parameters need not to be readjusted for varying operating conditions.

Instead of supplying the user with a certain value for the closed-loop amplification k_c as the best choice, limits for k_c were given which allow stable operation of the system. Depending on the desired changes in the terminal voltage amplitude the user himself can choose a value for k_c which satisfies his more specific requirements. One more constraint for the choice of k_c is the dynamic range of the power electronic converter. It would be useless to provide the converter with reference values of i^R which the converter is unable to supply to the rotor coils of the doubly-excited machine.

In the following a strategy for the choice of k_c is given which depends on two different operating conditions of the VSG system:

a) Maintenance of a certain terminal voltage:

In order to maintain a certain terminal voltage irrespective of varying power-demand conditions, k_c can be chosen close to the upper limit of stable operation. The VSG system then will be able to maintain the terminal voltage within an extremely narrow band. Fault conditions are left out of consideration at this point.

b) Response to required changes in the terminal voltage:

In order to respond to changing demands for the generation of reactive power the terminal voltage needs to be changed. Therefore k_c needs to be chosen small in order to allow stable transitions in the terminal voltage.

The response to demands for the generation of reactive power is the task of the supervisory controller. It would be possible to implement a logic to the supervisory controller that reduces k_c for the duration of the change in the terminal voltage. As soon as the new terminal voltage level is reached, k_c can be restored to its previous value. The implementation of this additional logic would allow the most efficient use of the voltage controller. The detection of fault conditions is another task of the supervisory controller.

While identifying the system transfer function, a numerical method called "Instrumental Variable Method" was used and proved to be extremely useful not only for the identification of the VSG system, but also for the identification of any other linear or nonlinear system. Moreover, the Instrumental Variable Method is easy to apply and provides information to verify the validity of the obtained results. The need for an auxiliary model $\bar{H}(z)$ proves to be no restriction at all since any other stable transfer function can be used. The user can apply the method iteratively starting with $\bar{H}(z) = 1$ and then insert for $\bar{H}(z)$ the transfer function as obtained in the previous calculation. This process needs to be repeated until the desired degree of approximation is reached. In this particular case it was straightforward to use the function G(s) as the auxiliary model since G(s) was already available as a relatively close approximation of the VSG system. An iterative calculation did not seem to yield substantial improvements.

During the course of determining the parameters for the controller the LOCIPRO software (BV - ENGINEERING, 1985) proved to be an useful tool to determine the root-locus of closed-loop systems. However, the possibility to implement parallel branches was not given in the software.

By increasing the order of the stabilizer polynomials, the quality of the dynamic behavior of the closed-loop system could have been improved. This is obviously at the cost of a more complex and therefore less reliable controller.

The verification process showed that the neglect of ω_m as a state variable in the electric system was justifyable at the cost of a less desirable dynamic behavior of the VSG system. However, taking ω_m into consideration again would have been at the cost of a more sophisticated controller.

The results demonstrate that the non-complex voltage controller as designed is effective over the entire range of operation of the VSG system. Moreover, the controller is capable of producing the desired speed of response as well as a minimal overshoot if the input is subjected to step changes.

BIBLIOGRAPHY

[1] Cycloconverter-Excited Divided-Winding Doubly-Fed Machine as a Wind-Power Converter, IEEE Proc., Volume 131, March 1984

[2] Characteristics of the doubly-fed machine in a hydro variable-speed generation system, Bonneville Power Administration, Contract No. 79-85BP24332, Progress report on Task (2), November 1985

[3] Stabilizing Control Strategies for the Doubly Excited Machine
Gerald A. Permantier, MS thesis,
Oregon State University 1984

[4] Digital Signal Processing
A.V. Oppenheim, R.W. Schafer
Prentice-Hall 1975

[5] Control System Engineering
Mohamed E. El-Hawary
Reston Publication Company 1984

[6] Modeling and Identification of dynamic systems
N.K. Sinha, B. Kuszta
Van Nostrand Reinhold electrical computer science and engineering series 1983

[7] Control Systems Theory
Olle I. Elgerd
McGraw-Hill 1967